UNIVERSITY OF CALIFORNIA,
IRVINE

Nanowire Spin Torque Oscillator Driven by Spin Orbit Torques

DISSERTATION

submitted in partial satisfaction of the requirements
for the degree of

MASTER OF SCIENCE

in Chemical and Material Physics

by

Andrew Smith

Dissertation Committee:
Professor Ilya Krivorotov, Chair
Assistant Professor Matt Law
Professor Peter Taborek

2016

TABLE OF CONTENTS

LIST OF FIGURES

ACKNOWLEDGMENTS

I would like to express my gratitude to my committee chair, Dr. Ilya Krivorotov, for allowing me to commence my journey of self discovery and scientific insight under his guidance. A half decade latter and I am still surprised by the breadth of his knowledge, intuition and leadership. I would also like to thank my committee members, Dr. Matt Law and Dr. Peter Taborek for taking time out of their busy schedules to help me accomplish this daunting task.

I would like to thank everyone that I had the pleasure to call a labmate over the years: Dr. Jian Zhu, Dr. Graham Rowlands, Dr. Zheng Duan, Dr. Igor Barsukov, Dr. Brian Youngblood, Dr. Liu Yang, Yu-Jin Chen, Han Kyu Lee, Jenru Chen, Jieyi Zhang, Alejandro Jara, Chris Safranski, Chengcen Sha, Dr. Eric Montoya, Josh Dill, Alexandre Goncalves, Riccardo Tomasello and Tobias Schneider. Whether it be scientific or social needs, there was always a helping hand. I would also like to thank my collaborators including Dr. Jurgen Linder, Dr. Vladislav E. Demidov, Dr. Sergej O. Demokritov, Dr. Roman Verba, Dr. Vasil Tiberkevich, Dr. Andrei N. Slavin, Dr. Rodrigo Arias and Kemal Sobotkiewich. I would like to thank the staff members of LEXI and INRF that have helped me fabricate and characterize samples throughout the years with special recognition to Dr. Qiyin Lin for your XRD expertise and Mo Kebaili, Jake Hes and Ryan Smith for all of the clean room assistance. I would like to acknowledge Nature Communications for allowing the use of "Nanowire spin torque oscillator driven by spin orbit torques" for chapter 3 of this dissertation.

I would also like to thank my friends and family for haboring my escape from grad school in times of need. Whether they were near or far, their love, support and joyfulness was always felt. Lastly, I would like to thank my girlfriend, Dr. Amanda Weber, for without her infectious brightness and unending support, this would not be possible. In the most stressful moments, you were always there to listen to me rant and encourage me to push through or take a step back and relax.

CURRICULUM VITAE

Andrew Smith

EDUCATION

Master of Science in Chemical and Materical Physics **2016**
University of California, Irvine *Irvine, California*

Bachelor of Science in Physics **2010**
Marquette University *Milwaukee, Wisconsin*

RESEARCH EXPERIENCE

Graduate Research Assistant **2011–2016**
University of California, Irvine *Irvine, California*

Undergraduate Research Assistant **2008–2009**
Marquette University *Milwaukee, Wisconsin*

TEACHING EXPERIENCE

Teaching Assistant **2010–2011**
University of California, Irvine *Irvine, California*

Teaching Assistant **2007–2010**
Marquette University *Milwaukee, Wisconsin*

REFEREED JOURNAL PUBLICATIONS

L. Yang, R. Verba, V. Tiberkevich, T. Schneider, **A. Smith**, et al. Reduction of phase noise in nanowire spin orbit torque oscillators. *Sci. Rep.* 5, 16942 (2015)

Z. Duan*, **A. Smith***, L. Yang*, B. Youngblood*, et al. Nanowire spin torque oscillator driven by spin orbit torques. *Nat. Commun.*. 5:5616 (2014)

Andrew Kunz, Eric C. Breitbach and **Andrew Smith**. Anti-vortex dynamics in magnetic nanostripes. *Journal of Applied Physics*. 105, 07D502 (2009)

REFEREED CONFERENCE PUBLICATIONS

Andrew Smith, Tobias Schneider, Liu Yang, Zheng Duan and Ilya N. Krivorotov. Dimensional crossover in spin Hall oscillators. *American Physics Society - March Meeting*. Oral (2016)

Andrew Smith, Tobias Schneider, Liu Yang, Zheng Duan and Ilya N. Krivorotov. Dimensional crossover in spin Hall oscillators. *Magnetism and Magnetic Materials*. Poster (2016)

Andrew Smith, Liu Yang, Brian Youngblood, Zheng Duan and Ilya N. Krivorotov. Time domain measurements of a spin torque oscillator driven by spin orbit torques. *Magnetism and Magnetic Materials*. Oral (2014)

Andrew Smith, Zheng Duan, Liu Yang, Brian Youngblood and Ilya N. Krivorotov. Nanowire spin torque oscillator driven by spin orbit torques. *American Physics Society - March Meeting*. Oral (2014)

ABSTRACT OF THE DISSERTATION

Nanowire Spin Torque Oscillator Driven by Spin Orbit Torques

By

Andrew Smith

Master of Science in Chemical and Material Physics

University of California, Irvine, 2016

Professor Ilya Krivorotov, Chair

The field of spintronics deals with the use of the spin degree of freedom of the electron and the spin current that arises from it. There are many static and dynamic applications for spin current whether it is supplied by spin polarized electric current from a magnetic layer or from spin orbit torques. This dissertation will focus on the later cases where the spin Hall effect present in platinum supplies a spin torque on an adjacent permalloy layer creating a spin torque oscillator(STO). Previous studies have demonstrated the existence of STOs in the 0-dimensional case and its absence in the 2D case therefore the 1D case, a ferromagnetic nanowire, is tackled here. This will cover the first instance of a micrometer scale STO and will show the excited modes are the edge and bulk spin wave eigenmodes of the nanowire.

Chapter 1

Introduction

Spintronics has become a hot topic in the scientific community for a reason. By utilizing the the spin degreee of freedom of an electron, new nanoscale devices are now possible such as STT-MRAM and logic gates. In metals with low spin orbit coupling (SOC), the spin of the electrons are orientated randomly resulting in only electric current. However, in magnetic or large SOC materials, the spins become polarized leading to both electric and spin current. These spin currents can then interact with other magnetic layers allowing for local manipulation of magnetic moments via spin transfer torque.

One such case is a spin torque oscillator (STO) where the Gilbert damping of a magnetic layer is cancelled out by the spin torque from a spin current which leads to self-oscillatory dynamics in the GHz range. These auto oscillators are among the smallest in the world (as small as 50 nm) and have garnered interest from industry for applications such as on chip local oscillators, associative memory blocks for image processing, nanoscale magnetic field sensing, logic devices and many more. Chapter 2 will cover the background material needed to understand the results of this work. Chapter 3 will go over what a nanowire spin Hall

oscillator is and the interesting role dimensionality plays in STO. Chapter 4 will conclude these thoughts.

Chapter 2

Background

2.1 Spin Transfer Torque

The concept of spin transfer torque was first proposed by Slonczewski[1] and Berger[2] in 1996. The phemoneom is best understand in the framework of exchange interactions between quasi-localized and conduction electrons as illustrated in Fig. 2.1. The local d electrons responsible for ferromagnetism of a material is initially at an energy minimum with its spin aligned with the local magnetic field. When a conduction electron that is polarized in a different direction than the local moment passes by, the two spins exert torque onto each other due to the exchange interaction. This will cause both electrons to deflect from their original directions which has two consenquences. The first is that the conduction electron will leave the site with the spin information of the local moment which can then interact with other local moments. Secondly, the local moment will now be shifted away from the energy minimum which will then relax back to its ground state.

If now there is a constant flow of electrons with the spins polarized along a given direction, then the local moment will be continuously kicked in that direction and will remain there

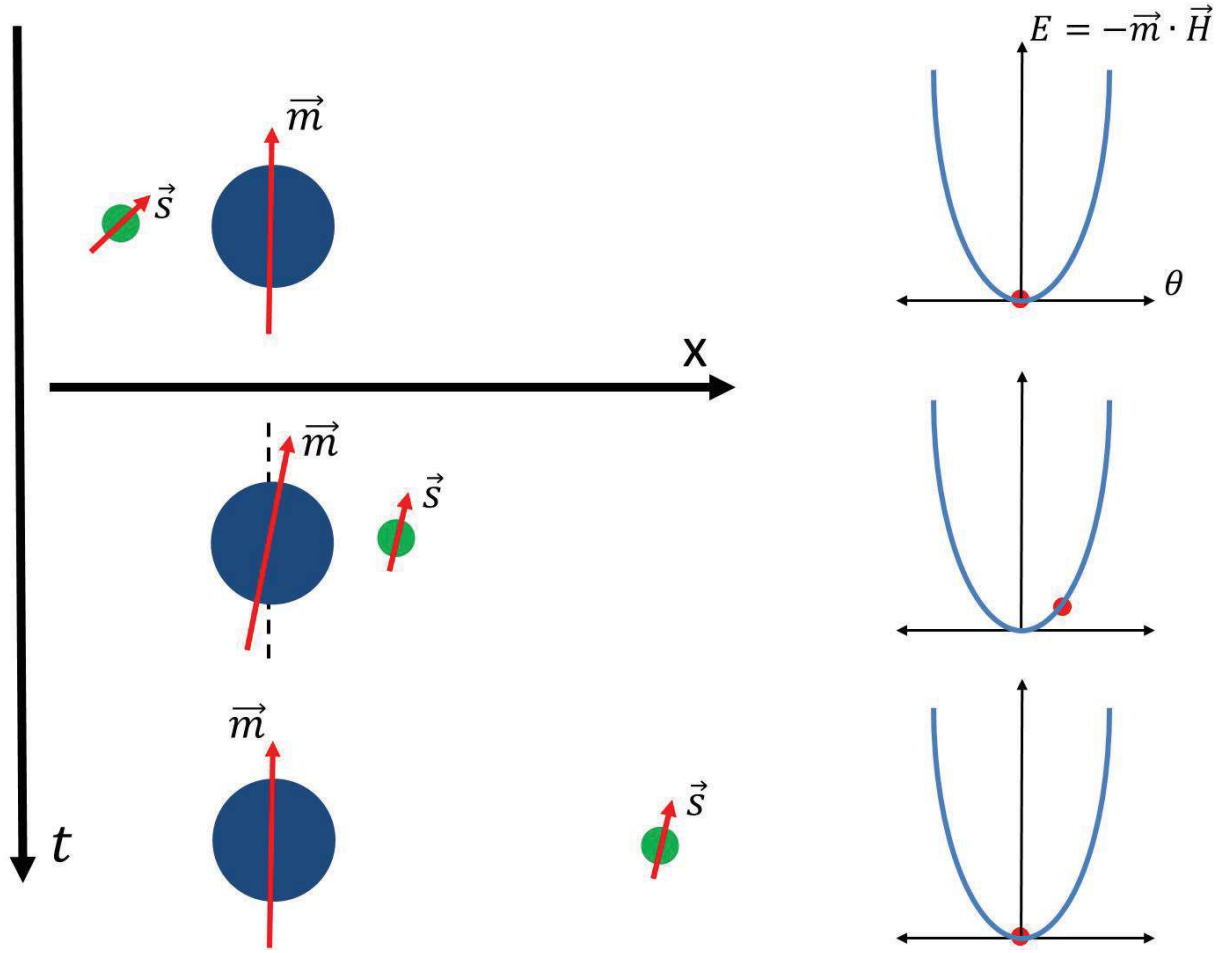

Figure 2.1: Illustration of spin torque where conduction electron and localized magnetic moment exert torques on each other which temporarly shifts the moment away from equalibrium.

as long as the current is present. Once the current is removed, the local moment will then return back to an energy minimum. In the case of a constant flow of electrons but the spins are polarized in random directions, then the local moment will be kicked around in random directions which average out to 0 leading to the moment staying aligned along the local magnetic field. In either case, this incident electric current will then be converted into electric and spin current with its polarization in the direction of the local moment which can then be used by a second ferromagnetic layer.

2.2 Sources of Spin Current

2.2.1 Spin Valve

The first sources of spin current, a spin valve, utilized a relatively thick reference ferromagnetic layer ($\sim$ 8 nm) called the fixed layer to spin polarize an electric current. This is then injected into a nonmagnetic spacer layer of similar thickness and then into a ferromagnetic layer of interest called the free layer which experiences a torque. Often times, the fixed layer consists of additional layers that help increase the coericive field in order to improve the stability of the fixed layer. The polarization effeciency (P) of the spin valve depends on the spin dependent band structure of the whole system. The intial polarization of the spins depends on the spin dependent density of states where if all of the conduction electrons are spin up, then P = 1 and if all of them are down, P = -1[3]. Then, the conduction electrons pass through the rest of the structure where spin flip and reflection events take place. These events predominately occur at interfaces and are governed by the band structure mismatch of dissimilar materials. The total polarization effeciency is then defined as the net spin current to charge current ratio that enters the free layer. This value is typically between 0.1-0.5 and is highly dependent on not only the ferromagnetic materials but also the spacer layer. If the metallic spacer layer is replaced with an insulating layer, an additional torque is present called the field like torque[4]. This is due to it now being a tunneling process which only involves select states on the Fermi surface. Therefore, a nonzero transverse component of the spin polarization is possible.

2.2.2 Spin Hall Effect

Recently, the spin Hall effect (SHE) and spin orbit coupling (SOC) has become of great interest in the spintronics community because of its ability to generate spin current without

the use of a ferromagnetic reference layer[5,6]. Instead of the ferromagnet, a material with strong SOC such as Platinum or Tantalum is used. Due to spin dependent scattering, a pure spin current is generated transverse to the injected electric current with its polarization transverse to both. The ratio of spin current to charge current is called the spin Hall angle (SHA) and can reach as high as 33 percent[7]. The physics describing the SHE is the same as for the anomalous Hall effect in ferromagnets which is described by both intrinsic and extrinsic contributions.

The intrinsic contribution results from the Berry phase accumulated as you sweep through k-space about the Fermi surface therefore this happens inbetween scattering events.[8–10] The Berry phase is maximized when SOC splits a band such that one spin orientation lies just below the fermi surface while the other just above such that their respective phases are not cancelled out[11]. This phase acts as an addition spin dependent transverse voltage to the applied voltage which deflects spins in different directions based on their spin orientation.

The extrinsic contribution is due to two mechanism both of which occur due to scattering events. The first is skew scattering where electrons with opposite spin are deflected in opposite directions due to the difference of the SOC of the host material and the impurity[12]. The second is side jump scattering where electrons of opposite spin are shifted instead of deflected in opposite directions[13]. This results in spin accumulation transverse to the applied voltage and may have a different sign as the intrinsic contribution.

2.3 Magnetoresistance

The use of magnetoresistance (MR) is critical in magnetics since it allows the magnetic state to be observed by electrical means. Without it, magnetic memory would have never became the mainstream research direction in the semiconductor industry. Although there are many

different types of magnetoresistances, the three that appear the most are anisotropic magnetoresistance (AMR), giant magnetoresistance (GMR), and tunneling magnetoresistance (TMR).

Anisotropic magnetoresistance, discovered in 1857 by Lord Kelvin, is an effect such that the resistance of the ferromagnetic layer depends on the orientation of the magnetization and the electric field where the resistance is maximum when the two are aligned and minimum when they are transverse[14]. This is due to increased s-d scattering in the direction of the magnetization from SOC. Although typical AMR ratios range from 0.5-5 percent in bulk materials and typically decreases with decreasing thickness, it only requires a single ferromagnetic layer unlike other commonly utilized magnetoresistances[15].

Giant magnetoresistance, a magnetoresistance so important that its discovers, Albert Fert and Peter Grnberg, were awarded a Nobel prize in 2007, relies on 2 magnetic layers seperated by a nonmagnetic metallic spacer layer[16,17]. The resistance of the overall structure depends on the angle between the 2 magnetizations and typically is minimum when they are parallel to each other and maximum when anti-parallel. The GMR ratio, which can be as high as 220 percent[18], depends on the band structure of all 3 layers and can best be understood as a simple 2 channel resistor problem, one for spin up and the other for spin down as illustrated in Fig. 2.2[19].

A spin up electron can more easily pass through a ferromagnetic material if it is also spin up due to the increased density of states (DOS) of the majority conduction band. On the other hand, if the ferromagnetic material is of opposite spin, there will be increased resistance as there is a lower DOS for the minority conduction band. Therefore, if both ferromagnetic layers are spin up, then the spin up electrons will easily pass through the structure while the spin down electrons are blocked. Eventually, these blocked spin down electrons will undergo a spin flip event and then be allowed to pass. This can be viewed as shorting out the circuit along the spin up channel. Now, if one layer is spin up, and the other is spin

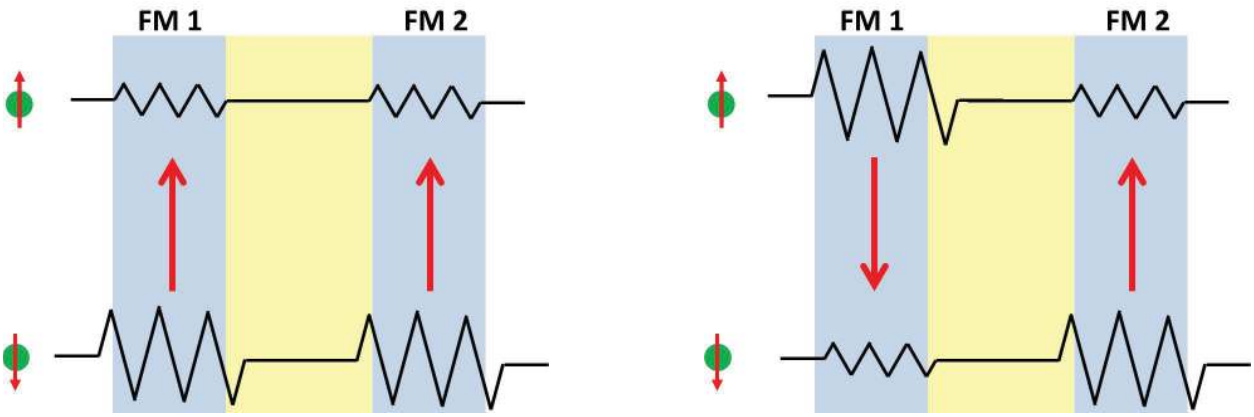

Figure 2.2: Diagram illustrating low resistance (left) and high resistance (right) states for giant magnetoresistance.

down, the electrons that can easily pass through one layer are blocked by the other. In this configuration, the circuit is no longer shorted so the resistance is higher.

Tunneling magnetoresistance is very similar to GMR however, instead of a metallic spacer layer, an insulating layer is used. Because of this, the electrons must tunnel across the insulating layer which greatly limits the available states for transport. Since tunneling is required, the non spin dependent transport is severly reduced which then allows for much higher MR ratios of up to 1144 percent[20]. Currently, TMR is used in read heads for hard drives and the building block for MRAM.

2.4 Structures

Although there are many different ways a device can take shape, there are three main categories that most belong in such that high current densities needed for spin torque manipulation are achieved. The first is the nanopillar structure as shown in Fig. 2.3(a) where there is a free layer and a spin valve that supplies the spin current. Both parts are patterned into a nanoscale structure (∼100 nm) and an electric current is applied vertically through the structure. This leads to a spin current in the same direction due to the spin valve which

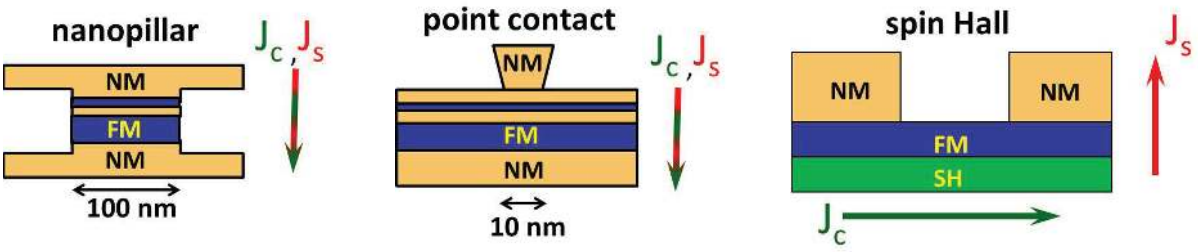

Figure 2.3: Illustrations of device geometries with electric current in green and spin current in red for (a) nanopillar, (b) point contact and (c) spin Hall structures.

then manipulates the free layer. In order to read the state, GMR or TMR is used depending on the spacer layer.

The second structure is the point contact configuration as shown in Fig. 2.3(b) and is very similar to the nanopillar. Instead of patterning the free layer and the spin value, it is left as a thin film. In order to provide the high current densities needed for applications, a very small (∼10 nm) nonmagnetic contact is fabricated ontop of the film. The dynamics of these structures differs from nanopillar devices due the interactions between the magnetization under the point contact and the rest of the film.

The third structure called the spin Hall geometry shown in Fig. 2.3(c) is unlike the other two. Instead of a spin valve, a spin Hall (SH) material such as Platinum is used. Electric current is then applied longitudinally through the FM and SH layers which injects spin current vertically into the FM. The state of the magnetization can then be determined through AMR instead of GMR or TMR since there is only one magnetic layer. Even though the magnetoresistance of this structure type is smaller compared to the vertical current counterparts, it has exploded in popularity due to the ease of fabrication along with the polarization of the spin current always being normal to the flow of the electric current.

2.5 Magnetization Dynamics

How magnetization responds to magnetic fields is described by the Landua Lifshitz (LL) equation[21,22].

$$\frac{d\mathbf{m}}{dt} = -\gamma\left(\mathbf{m}\times\mathbf{H}_{eff} + \alpha\mathbf{m}\times\mathbf{m}\times\mathbf{H}_{eff}\right) \tag{2.1}$$

This equation shows that a magnetic moment in the presence of a magnetic field will experience two torques. The first is the conservative field torque that causes the moment to process about the field direction. The second is a non-conservative damping torque that aligns the moment with the magnetic field direction. This means, when a moment isn't aligned with the magnetic field, the moment will oscillate as its time averaged component moves towards the field direction. Once the time averaged moment is aligned, the oscillation will decay away leading to static magnetization in the direction of the field.

$$\frac{d\mathbf{m}}{dt} = -\gamma\left(\mathbf{m}\times\mathbf{H}_{eff} + \alpha\mathbf{m}\times\mathbf{m}\times\mathbf{H}_{eff} + \beta\mathbf{m}\times\mathbf{m}\times\mathbf{p} + \beta'\mathbf{m}\times\mathbf{p}\right) \tag{2.2}$$

$$\beta = \left|\frac{\hbar}{\mu_o e}\right|\frac{J}{dM_s}\frac{P\Lambda^2}{(\Lambda^2+1)+(\Lambda^2-1)(\mathbf{m}\cdot\mathbf{p})} \qquad \beta' = const*\beta$$

If now spin current is present, two more addition torques get added to Eq. (2.1) called the Slonczewski terms which leads to Eq. (2.2)[1]. Again, there is a field like torque and a non conservative damping like torque resulting from the spin current where the polarization direction replaces the field direction. Generally, the field like torque is small and is often omited except for magnetic tunnel junction devices. The damping like torque however, allows for a lot of different phenomena as it can modulate the effective magnetic damping in the system. If the spin torque is large enough, it can overcome the magnetic damping in the system and rotate the magnetization away from the magnetic field direction as discussed in section 2.1. Solving Eq. (2.2) is fundamental to understanding all types of magnetic

phenomena ranging from switching a magnetic element to exciting GHz frequency auto-oscillations.

2.5.1 Micromagnetics

A useful tool for understanding experimental data is micromagnetics which involves breaking up a layer of magnetic material into cells the size of the exchange length (λ_{exch}) and solving the LLG equation. The most common micromagnetic software is Object Orientated Micromagnetic Framework (OOMMF) developed by NIST which is open source and CPU based[23]. Micromagnetics is heavely used for studying ferromagnetic layers because neighboring atomic spins are parallel to each other due to the exchange interaction being the dominate energy. This allows for an intermediate characterisitc length scale ($\lambda_{exch} \sim 5$ nm) to be used that has a manageable number of sites (magnetic moments) compared to atomic scale such that the LLG equation can be numerically calculated. At this scale, other energies become more relavent which can rotate the magnetization of one cell away from another cell leading to spatially varying magnetization profiles.

$$E = E_{exch} + E_{demag} + E_{anis} + E_{ext} \tag{2.3}$$

$$\mathbf{H}_{eff} = -\frac{\partial E}{\partial \mathbf{m}} \tag{2.4}$$

The energy of a magnetic moment is described by Eq. (2.3) and the effective magnetic field resulting from this energy is described by Eq. (2.4). The first term is the exchange energy which, as discussed earlier, trys to keep neighboring moments aligned with each other in a ferromagnet. The second term is the demagnetization energy which trys to align the magnetization along the surfaces in order to reduce surface magnetic charges which results in a curvature of the magnetization. The competetion between these two energies provide the main contributions to the curl of the magnetization. The third term is the anisotropy

energy which tries to align the magnetization along a perfered axis or plane. The sources for this energy are many, but they can all be characterized as either volumetric or interfacial. The last term is due to an external magnetic field being applied to the sample and tries to align the moment to this field. Therefore, the process for micromagnetics is to calculate the energy for the current magnetization state using Eq. (2.3), use that to calculate the magnetic field using Eq. (2.4), which is then plugged into Eq. (2.2) and calculated for a small timestep which then produces a new magnetic state. This then is repeated until $\frac{d\mathbf{m}}{dt}$ is below a threshold such that an energy minimum is found or a certain amount of time has passed.

2.5.2 Spin Waves

A spin wave is a disturbance in the magnetic order that is also a eigenmode of the magnetic system. The simpliest form is a plane wave solution such that it can be written as an oscillation of the magnetic moment about a time independent equalibrium magnetization ($\mathbf{m}_\mathrm{o}$).

$$\mathbf{m}(\mathbf{r},t) = \mathbf{m}_\mathrm{o} + \Delta\mathbf{m}(\mathbf{r})e^{i(\mathbf{k}\cdot\mathbf{r}-\omega t)} \tag{2.5}$$

The frequency of a spin wave is in the GHz regime where its wavelength is tied to its frequency through the magnetic field dependent dispersion relation of the system. The particle version of a spin wave is called a magnon which is analogous to phonons for lattice vibrations. The easiest example of a spin wave can be seen in a 1D chain of magnetic moments as shown in Fig. 2.4 with a wavelength of five moments. The equalibrium magnetization is set by the static local field, $\mathbf{H}$, and then an external force perturbs the system which excites the spin wave. This excitation can be caused by various methods but the most common are thermal,

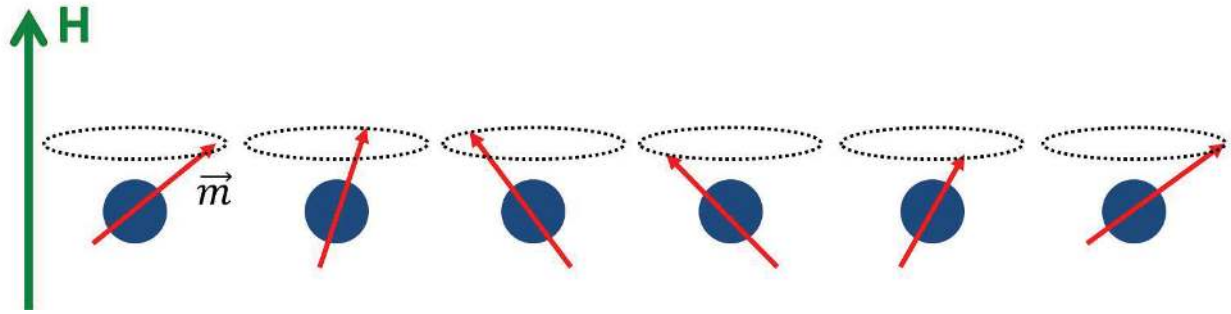

Figure 2.4: Spin wave with a wavelength of 5 magnetic moments in a 1D chain.

which is frequency indepedent, or a GHz frequency torque, either an AC magnetic field or spin torque.

2.5.3 Spin Torque Ferromagnetic Resonance

Spin torque ferromagnetic resonance (ST-FMR) is a useful tool for measuring the spin wave eigenmodes of a nanowire. By applying an AC spin torque into a ferromagnetic layer, spin waves are resonantly excited when the injected frequency matches an eigenfrequency of the magnetic system. When a spin wave is excited, the magnetization will oscillate which generates a resistance oscillation due to the magnetoresistance present in the device at the frequency of the spin wave or its harmonics. This resistance oscillation will rectify the injected electric current generating a DC voltage[24,25].

$$V = V_{PR} + V_{PV} = I_{dc}R_{dc} + I_{ac}\delta R_{ac}\cos\phi \tag{2.6}$$

Therefore, there will be either peaks or dips in the DC voltage depending on the phase difference whenever a spin wave mode is excited. In order to see these extremas, whose linewidth is proportional to the damping of the mode, either the injected frequency or the applied magnetic field is held fixed while the other is swept.

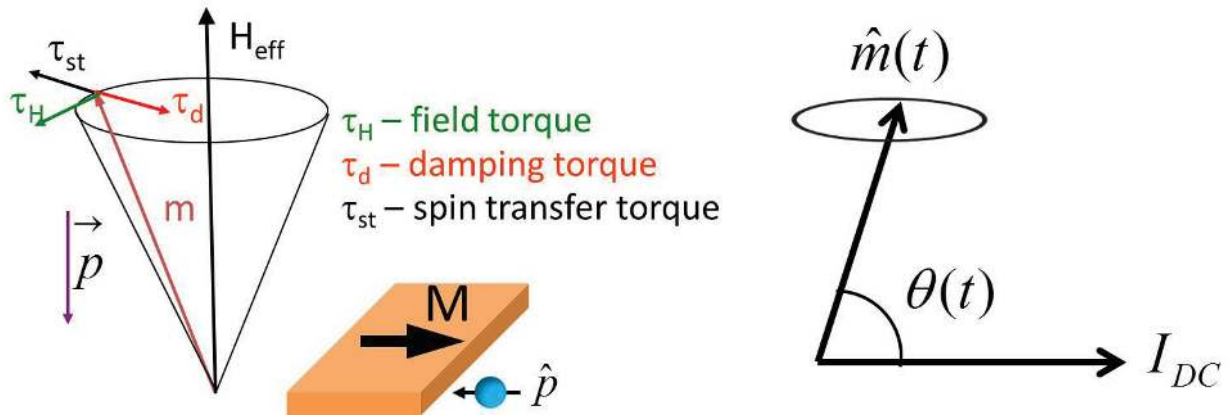

Figure 2.5: llustration of the canceling damping like torques leading resulting in self-oscillations (left) which produces an AC voltage due to the oscillating resistance (right).

2.5.4 Spin Torque Oscillators

Spin torque oscillators (STO) are one of the more unusual outcomes between the competition of the damping torques from an applied magnetic field and the presence of spin current. If the polarzation of the spin current has a component that is anti-parallel to the magnetic field direction as illustrated in Fig. 2.5, then the damping like torque from the spin current acts as negative damping and can cancel out the damping torque from the field. If they are of equal magnitude, then the conservative torque will cause the magnetic moment to oscillate about the equalibrium magnetization direction along a constant energy trajectory. This is an auto-oscillatory state whose frequency is determined by the eigenmode frequency of the excited state[26]. Typically, a self-localized bullet mode is excited whose frequency is below the spin wave spectrum, however, spin waves can be excited in certain geometries. These magnetic oscillations will then produce an AC voltage due to the oscillating resistance and the DC electric current which can then be detected with a spectrum analyzer.

Bibliography

[1] J.C. Slonczewski. "Current-driven excitation of magnetic multilayers". In: *Journal of Magnetism and Magnetic Materials* 159.1-2 (1996), pp. L1–L7. DOI: doi:10.1016/0304-8853(96)00062-5. URL: http://dx.doi.org/10.1016/0304-8853(96)00062-5.

[2] L. Berger. "Emission of spin waves by a magnetic multilayer traversed by a current". In: *Phys. Rev. B* 54.13 (1996), pp. 9353–9358. DOI: http://dx.doi.org/10.1103/PhysRevB.54.9353. URL: http://dx.doi.org/10.1103/PhysRevB.54.9353.

[3] Mark Johnson and R. H. Silsbee. "Interfacial charge-spin coupling: Injection and detection of spin magnetization in metals". In: *Phys. Rev. Lett.* 55.17 (1985), pp. 1790–1793. DOI: http://dx.doi.org/10.1103/PhysRevLett.55.1790. URL: http://dx.doi.org/10.1103/PhysRevLett.55.1790.

[4] J. C. Slonczewski. "Conductance and exchange coupling of two ferromagnets separated by a tunneling barrier". In: *Phys. Rev. B* 39.10 (1989), pp. 6995–7002. DOI: http://dx.doi.org/10.1103/PhysRevB.39.6995. URL: http://dx.doi.org/10.1103/PhysRevB.39.6995.

[5] D'yakonov M.I. and Perel' V. I. "Possibility of Orienting Electron Spins with Current". In: *Sov. Phys. JETP Lett.* 13.11 (1971), p. 467. URL: http://www.jetpletters.ac.ru/ps/1587/article_24366.pdf.

[6] J. E. Hirsch. "Spin Hall Effect". In: *Phys. Rev. Lett.* 83.9 (1999), pp. 1834–1837. DOI: http://dx.doi.org/10.1103/PhysRevLett.83.1834. URL: http://dx.doi.org/10.1103/PhysRevLett.83.1834.

[7] Chi-Feng Pai et al. "Spin transfer torque devices utilizing the giant spin Hall effect of tungsten". In: *Appl. Phys. Lett.* 101.12 (2012), p. 122404. DOI: http://dx.doi.org/10.1063/1.4753947. URL: http://dx.doi.org/10.1063/1.4753947.

[8] T. Jungwirth, Qian Niu, and A. H. MacDonald. "Anomalous Hall Effect in Ferromagnetic Semiconductors". In: *Phys. Rev. Lett.* 88.20 (2002). DOI: http://dx.doi.org/10.1103/PhysRevLett.88.207208. URL: http://dx.doi.org/10.1103/PhysRevLett.88.207208.

[9] G. Y. Guo et al. "Intrinsic Spin Hall Effect in Platinum: First-Principles Calculations". In: *Phys. Rev. Lett.* 100.9 (2008). DOI: http://dx.doi.org/10.1103/PhysRevLett.100.096401. URL: http://dx.doi.org/10.1103/PhysRevLett.100.096401.

[10] T. Tanaka et al. "Intrinsic spin Hall effect and orbital Hall effect in 4 d and 5 d transition metals". In: *Phys. Rev. B* 77.16 (2008). DOI: http://dx.doi.org/10.1103/PhysRevB.77.165117. URL: http://dx.doi.org/10.1103/PhysRevB.77.165117.

[11] Axel Hoffmann. "Spin Hall Effects in Metals". In: *IEEE Trans. Magn.* 49.10 (2013), pp. 5172–5193. DOI: 10.1109/TMAG.2013.2262947. URL: http://dx.doi.org/10.1109/TMAG.2013.2262947.

[12] J. Smit. "The spontaneous hall effect in ferromagnetics {II}". In: *Physica* 24.15 (1958), pp. 39 –51. ISSN: 0031-8914. DOI: http://dx.doi.org/10.1016/S0031-8914(58)93541-9. URL: http://www.sciencedirect.com/science/article/pii/S0031891458935419.

[13] L. Berger. "Side-Jump Mechanism for the Hall Effect of Ferromagnets". In: *Phys. Rev. B* 2.11 (1970), p. 4559. URL: https://journals.aps.org/prb/pdf/10.1103/PhysRevB.2.4559.

[14] W. Thomson. "On the electro-dynamic qualities of metals: Effects of magnetization on the electric conductivity of nickel and iron". In: *Proc. Roy. Soc* 8 (1857), pp. 546–550.

[15] T. McGuire and R. Potter. "Anisotropic magnetoresistance in ferromagnetic 3d alloys". In: *IEEE Trans. Magn.* 11.4 (1975), pp. 1018–1038. DOI: 10.1109/TMAG.1975.1058782. URL: http://dx.doi.org/10.1109/TMAG.1975.1058782.

[16] M. N. Baibich et al. "Giant Magnetoresistance of (001)Fe/(001)Cr Magnetic Superlattices". In: *Phys. Rev. Lett.* 61.21 (1988), pp. 2472–2475. DOI: http://dx.doi.org/10.1103/PhysRevLett.61.2472. URL: http://dx.doi.org/10.1103/PhysRevLett.61.2472.

[17] G. Binasch et al. "Enhanced magnetoresistance in layered magnetic structures with antiferromagnetic interlayer exchange". In: *Phys. Rev. B* 39.7 (1989), pp. 4828–4830. DOI: http://dx.doi.org/10.1103/PhysRevB.39.4828. URL: http://dx.doi.org/10.1103/PhysRevB.39.4828.

[18] R. Schad et al. "Giant magnetoresistance in Fe/Cr superlattices with very thin Fe layers". In: *Appl. Phys. Lett.* 64.25 (1994), p. 3500. DOI: 10.1063/1.111253. URL: http://dx.doi.org/10.1063/1.111253.

[19] A. Fert and I. A. Campbell. "Two-Current Conduction in Nickel". In: *Phys. Rev. Lett.* 21.16 (1968), pp. 1190–1192. DOI: http://dx.doi.org/10.1103/PhysRevLett.21.1190. URL: http://dx.doi.org/10.1103/PhysRevLett.21.1190.

[20] S. Ikeda et al. "Tunnel magnetoresistance of 604% at 300 K by suppression of Ta diffusion in CoFeBMgOCoFeB pseudo-spin-valves annealed at high temperature". In: *Appl. Phys. Lett.* 93.8 (2008), p. 082508. DOI: http://dx.doi.org/10.1063/1.2976435. URL: http://dx.doi.org/10.1063/1.2976435.

[21] L. Landau and E. Lifshits. "On the theory of the dispersion of magnetic permeability in ferromagnetic bodies". In: *Physik. Zeits. Sowjetunion* 8 (1935), pp. 153–169.

[22] T.L. Gilbert. "Classics in Magnetics A Phenomenological Theory of Damping in Ferromagnetic Materials". In: *IEEE Trans. Magn.* 40.6 (2004), pp. 3443–3449. DOI: 10.1109/TMAG.2004.836740. URL: http://dx.doi.org/10.1109/TMAG.2004.836740.

[23] M.J. Donahue and D.G. Porter. *OOMMF User's Guide, Version 1.0*. Interagency Report NISTIR 6376. Gaithersburg, MD: National Institute of Standards and Technology, 1999.

[24] A. A. Tulapurkar et al. "Spin-torque diode effect in magnetic tunnel junctions". In: *Nature* 438.7066 (2005), pp. 339–342. DOI: 10.1038/nature04207. URL: http://dx.doi.org/10.1038/nature04207.

[25] J. C. Sankey et al. "Spin-Transfer-Driven Ferromagnetic Resonance of Individual Nanomagnets". In: *Phys. Rev. Lett.* 96.22 (2006). DOI: http://dx.doi.org/10.1103/PhysRevLett.96.227601. URL: http://dx.doi.org/10.1103/PhysRevLett.96.227601.

[26] S. I. Kiselev et al. "Microwave oscillations of a nanomagnet driven by a spin-polarized current". In: *Nature* 425.6956 (2003), pp. 380–383. DOI: 10.1038/nature01967. URL: http://dx.doi.org/10.1038/nature01967.

Chapter 3

Nanowire spin torque oscillator driven by spin orbit torques

When spin torque from a spin current is applied to a nanoscale region of a ferromagnet, it can act as negative magnetic damping resulting in the excitation of self-oscillations of the magnetization resulting in a 0D spin torque oscillator (STO). In contrast, if the spin torque is uniformly applied to an extended ferromagnet (2D), then the self-oscillatory state is not excited, but rather leads to a reduction of the saturation magnetization. This chapter reports the studies on the effect of spin torque in a nanowire which is an intermediate dimensionality (1D)[27]. Coherent self-oscillations of magnetization are observed in a ferromagnetic nanowire which serves as the active area of a STO driven by spin orbit torques. This work demonstrates that STOs can be excited in 1D systems and can exceed sizes beyond the nanometer length scale.

3.1 Introduction

A current of spin angular momentum incident on a ferromagnet exerts torque on its magnetization and drives it out of equilibrium[1,2]. Owing to its non-conservative nature, this spin torque (ST) can act as effective negative magnetic damping and thereby excite magnetization self-oscillations[26,28]. Spin torque oscillators (STO) have been realized in nanoscale spin valves[26,29–31], point contacts to magnetic multilayers[32–34] and nanoscale magnetic tunnel junctions[35–39]. Recently, a new type of STO based on current-induced spin orbit torques in a Permalloy(Py)/platinum(Pt) bilayer was demonstrated[40–42]. Spin orbit torques[43–45] in this system can arise from the spin Hall effect in Pt[5,6,11,46–49] and the Rashba effect at the Pt/Py interface[50–53].

In all STOs studied previously, the active region where the negative ST damping exceeds the positive Gilbert damping of the ferromagnet was restricted to nanoscale dimensions. A recent study[54] of spatially uniform ST applied to an extended ferromagnetic film revealed that coherent self-oscillations of magnetization cannot be excited in this two-dimensional (2D) magnetic system. Instead, spin torque was shown to significantly reduce the saturation magnetization of the film[54]. The absence of ST-driven self-oscillations in a 2D ferromagnet was attributed to amplitude-dependent damping arising from nonlinear magnon scattering that prevents any of the multiple interacting spin wave modes of the system from reaching the state of large amplitude self-oscillations. As a result, the energy and angular momentum pumped by ST into the film is redistributed among a large number of spin wave modes leading to reduction of the saturation magnetization of the film. This study raises an important question on the role of the magnetic system dimensionality in ST-induced magnetization dynamics.

In this chapter, it is demonstrated that spatially uniform ST can excite self-oscillations of magnetization in a one-dimensional (1D) magnetic system – a ferromagnetic nanowire.

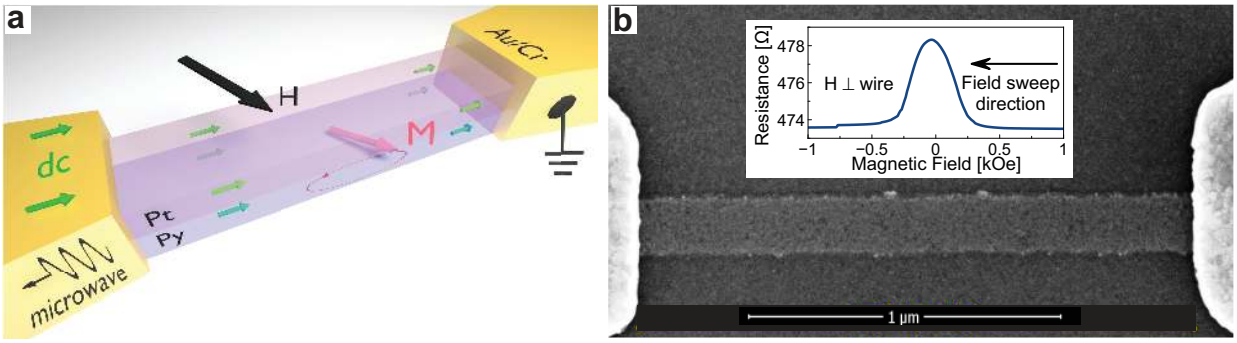

Figure 3.1: (a) Schematic of a Pt/Py nanowire STO device. (b) Scanning electron micrograph of the Pt/Py nanowire STO. The inset shows resistance versus in-plane magnetic field applied perpendicular to the nanowire measured at $T_b = 4.2$ K and a bias current of 0.5 mA.

Studies of ST-driven dynamics in a Pt/Py bilayer nanowire are covered, in which SO torques excite self-oscillations of magnetization over a 1.8 μm long active region. This nanowire STO exhibits two types of self-oscillatory modes that directly arise from the edge and bulk spin wave eigenmodes of the Py nanowire. This chapter suggests that geometric confinement of the spin wave spectrum in the 1D nanowire geometry limits the phase space for nonlinear magnon scattering compared to the 2D film geometry and thereby enables STOs with a spatially extended active region.

3.2 Results

3.2.1 Sample description

The nanowire STO devices studied in this work are patterned from Pt(5 nm)/Py≡$Ni_{80}Fe_{20}$(5 nm)/AlO_x(4 nm)/(GaAs substrate) multilayers deposited by magnetron sputtering. Multilayer nanowires that are 6 μm long and 190 nm wide are defined via e-beam lithography and Ar plasma etching. Two Au(35 nm)/Cr(7 nm) leads are attached to each nanowire with a 1.8 μm gap between the leads, which defines the active region of the device as shown in Fig. 3.1. The resistance of the device measured at bath temperature $T_b = 4.2$ K versus magnetic

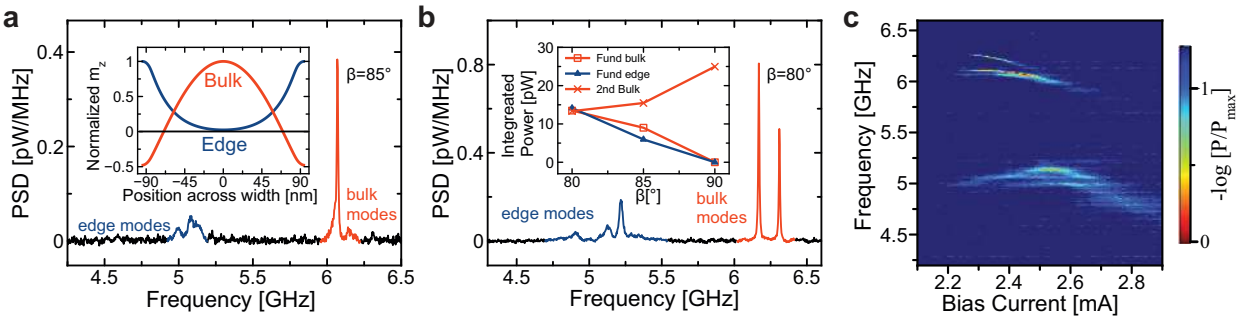

Figure 3.2: Power spectral density (PSD) of the microwave signal emitted by the nanowire at direct current bias $I_{dc} = 2.45$ mA, bath temperature $T_b = 4.2$ K and magnetic field $H = 890$ Oe applied in the plane of the sample at an angle (a) $\beta = 85°$ and (b) $\beta = 80°$ with respect to the nanowire axis. (c) Dependence of the emission spectrum on I_{dc} for $H = 890$ Oe and $\beta = 85°$. The inset in (a) shows the spatial profiles of the edge and bulk spin wave modes across the nanowire width given by micromagnetic simulations. The inset in (b) shows angular (β) dependence of the integrated power in the fundamental and the second harmonic of the bulk and edge groups of spectral peaks measured at $I_{dc} = 2.4125$ mA and $H = 890$ Oe.

field applied in the sample plane perpendicular to the nanowire is shown in the inset of Fig. 3.1. This plot reveals that the anisotropic magnetoresistance (AMR) of the Pt/Py bilayer is 1 %.

3.2.2 Electrical measurements

To study self-oscillatory magnetic dynamics excited by SO torques, a saturating magnetic field ($H > 0.5$ kOe) is applied in the plane of the sample in a direction nearly perpendicular to the nanowire axis. In this configuration, SO torques applied to the Py magnetization act as effective magnetic damping[47]. Direct current bias I_{dc} is applied to the nanowire and the microwave signal emitted by the device is measured using a spectrum analyzer[26]. The microwave signal $V_{ac} \sim I_{dc}\delta R_{ac}$ is generated by the AMR resistance oscillations δR_{ac} arising from the magnetization self-oscillations[42]. Microwave signal emission, shown in Fig. 3.2, is only observed above a critical current I_c with the current polarity corresponding to SO

torques acting as negative damping[47]. The microwave emission is measured for five nominally identical devices and similar results for all these samples is found.

For all samples, the microwave emission spectra for $I_{dc} > I_c$ exhibit two groups of closely spaced peaks with a frequency gap between the groups of ∼1 GHz. Each group consists of 1 to 4 distinct emission peaks separated from each other by tens of MHz. The high and low frequency groups of peaks appear at similar critical currents. Both groups of peaks are observed in the entire range of magnetic fields (H = 0.5 – 1.5 kOe) employed in this study. For the high frequency group of peaks, microwave emission is observed not only at the fundamental frequency shown in Fig. 3.2, but also at the second harmonic. As illustrated in the inset of Fig. 3.2(b), the emitted power at the fundamental frequency is zero for magnetic field applied at an angle $\beta = 90°$ with respect to the nanowire axis and increases with decreasing β. In contrast, the emitted power in the second harmonic has a maximum at $\beta = 90°$ and decreases with decreasing β. Such angular dependence of the emitted power in the fundamental and second harmonic is expected for a microwave signal arising from AMR. For the low frequency group of peaks, no emission is seen at the second harmonic, which can be explained by the smaller amplitude of magnetization precession reached by these modes and an equilibrium magnetization direction within the mode excitation area being closer to the nanowire axis. Fig. 3.2(c) illustrates the dependence of the emission spectra on I_{dc} for $H = 890$ Oe and $\beta = 85°$.

In order to determine the origin of the microwave emission signals, measurements of the spectrum of spin wave eigenmodes of the nanowire using spin torque ferromagnetic resonance (ST-FMR) is performed[24,25,55]. In this technique, a microwave current I_{ac} applied to the nanowire excites magnetization dynamics in Py by the combined action of current-induced SO torques and the Oersted field from the current in Pt, and thereby generates AMR resistance oscillations at the frequency of the microwave drive[55]. Mixing of the current and resistance oscillations as well as variation of the time-averaged sample resistance in response

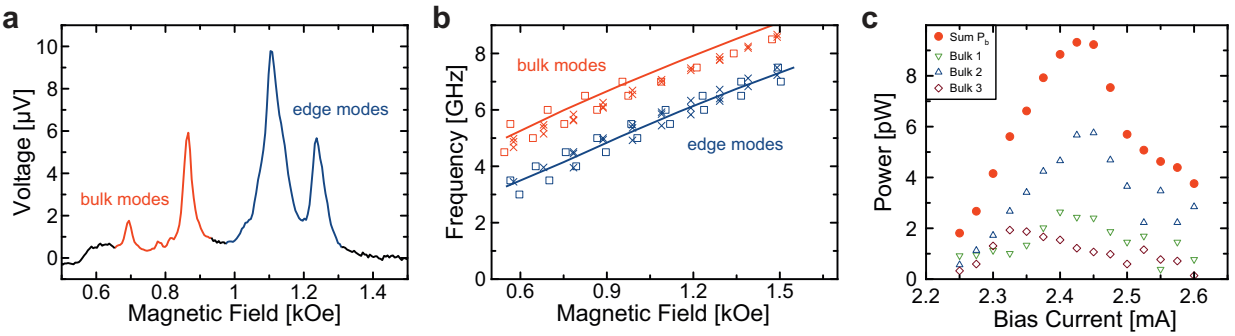

Figure 3.3: (a) ST-FMR spectrum of the nanowire device measured at the microwave drive frequency of 6 GHz, $\beta = 85°$ and $I_{dc} = 2.0$ mA $< I_c$. (b) Frequency versus magnetic field applied at $\beta = 85°$: (squares) spin wave eigenmodes measured by ST-FMR, (crosses) self-oscillatory modes at I_c and (lines) bulk and edge spin wave eigenmodes given by micromagnetic simulations for an ideal nanowire. (c) Bias current dependence of the integrated emitted power in individual peaks of the bulk group of self-oscillatory modes (open symbols) as well as the sum of integrated powers of all bulk modes P_b (crosses).

to the microwave drive[56,57] give rise to a direct voltage V_{dc} that is measured as a function of magnetic field H applied to the sample. Peaks in $V_{dc}(H)$ arise from resonant excitation of spin wave eigenmodes of the nanowire. An ST-FMR spectrum of spin wave eigenmodes measured at $\beta = 85°$, drive frequency of 6 GHz and $I_{dc} = 2.0$ mA $< I_c$ is shown in Fig. 3.3(a).

Similar to the microwave emission spectra, two groups of modes in the ST-FMR spectra are observed. In Fig. 3.3(b), the field dependence of the eigenmode frequencies measured by ST-FMR at $I_{dc} < I_c$ to the frequencies of self-oscillatory modes measured at I_c is compared. This figure demonstrates that the frequencies of all self-oscillatory modes at I_c coincide with the frequencies of spin wave eigenmodes of the system measured by ST-FMR. Therefore, all self-oscillatory modes of the system arise directly from spin wave eigenmodes of the nanowire. This type of eigenmode self-oscillation is qualitatively different from the spin wave bullet mode excited by SO torques in a planar point contact to an extended ferromagnetic film[40]. The bullet mode is a nonlinear type of oscillation, self-localized to a region with dimensions below 100 nm and with frequency below the spectrum of spin wave eigenmodes of the film[58].

It is well known that spin wave eigenmodes of a transversely magnetized thin-film ferromagnetic nanowire can be classified as bulk and edge eigenmodes[59–61]. These eigenmodes have spatially inhomogeneous profiles along the wire width with reduced (enhanced) amplitude near the wire edges for the bulk (edge) eigenmodes. The frequencies of the edge spin wave modes lie below those of the bulk modes due to reduced internal magnetic field near the wire edges[59]. The frequencies of all eigenmodes are sensitive to the values of magnetic parameters of the Py film, which are different from their bulk values due to the influence of proximate nonmagnetic layers. In addition, the frequencies of the edge modes depend on the edge roughness and spatial variation of the film magnetic properties (magnetic dilution) at the nanowire edges induced by etching[61].

The future section 3.2.4 describes how micromagnetic[23] fitting of three sets of experimental data: (i) wire resistance versus in-plane magnetic field, (ii) wire resistance versus out-of-plane magnetic field and (iii) quasi-uniform spin wave mode frequency versus magnetic field applied parallel to the wire axis can be used to determine the values of saturation magnetization M_s= 608 emu/cm^3, surface magnetic anisotropy $K_s = 0.237$ erg/cm^2 and edge dilution depth $D = 10$ nm, where D is defined as the distance from the wire edge over which magnetization linearly increases from zero to the full film value[61]. These values of M_s, K_s and D are consistent with previous studies of thin Py nanomagnets[62–64]. Using these values of the nanowire magnetic parameters and assuming translational invariance along the nanowire axis, micromagnetic simulations are performed to find the spectrum of spin wave eigenmodes for magnetic field applied in the sample plane at $\beta = 85^\circ$ discussed in section 3.2.4. This shows that the two lowest frequency spin wave modes are the edge and bulk modes, whose spatial profiles (defined as normalized out-of-plane amplitude of dynamic magnetization m_z) across the wire width are shown in the inset of Fig. 3.2(a). The frequencies of these two modes versus in-plane magnetic field are shown in Fig. 3.3(b).

It is clear from Fig. 3.3(b) that the frequencies of the calculated edge (bulk) modes are similar to the low (high) frequency groups of eigenmodes measured by ST-FMR and observed in STO measurements. This shows that the high (low) frequency groups of experimentally observed eigenmodes are closely related to the bulk (edge) eigenmodes of an ideal nanowire with translational invariance along the nanowire axis. Quantization along the wire results in splitting of the ideal nanowire eigenmode peaks, consistent with the experimentally observed fine frequency splitting within the high- and low-frequency groups of eigenmodes. The validity of this interpretation of the origin of the fine mode splitting, as opposed to e.g. symmetry breaking due to structural disorder of the wire edges, is demonstrated by the spatially resolved BLS data shown in Fig. 3.5(b) in section 3.2.3. Fig. 3.3(c) shows the dependence of the integrated microwave power emitted by the STO device on direct bias current I_{dc} for the three spectral peaks comprising the bulk group. The sum of the integrated powers in the three peaks versus I_{dc} is shown as well. Although the power in each individual peak exhibits irregularities as a function of I_{dc}, the sum of integrated powers of the entire group of bulk peaks is a smooth function of I_{dc}. This further suggests that the finely spaced peaks within the group arise from the splitting of a single peak by longitudinal quantization. The same trend is found for the edge group of peaks.

The precession cone angle θ_b achieved by the bulk mode in the self-oscillatory regime is estimated by assuming that the oscillation profile is approximately uniform along the wire length and define θ_b as the maximum angle of deviation of the magnetization from its equilibrium direction. θ_b is calculated by equating the experimentally measured integrated power in the bulk group of peaks P_b to the integrated power generated by the bulk mode of amplitude θ_b in an ideal nanowire as shown in section 3.2.5. This analysis shows that the maximum precession cone angle $\theta_b \approx 19^\circ$ is achieved at I_{dc} =2.425 mA. Although this value of θ_b is only an approximate estimate, it clearly shows that large precession cone angles are achieved in the auto-oscillatory regime. The maximum precession cone angle of the edge mode is estimated to be $\theta_e \approx 14^\circ$. The large values of the integrated power emitted by the nanowire

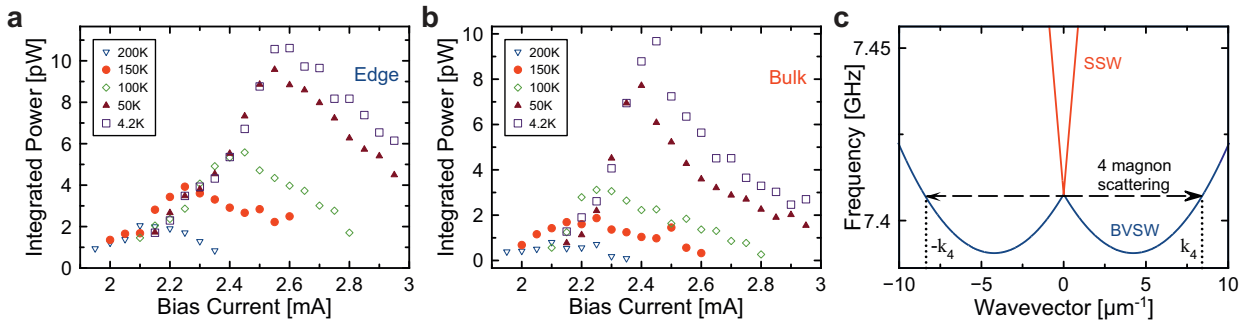

Figure 3.4: Bias current dependence of the integrated microwave power emitted by the bulk (a) and edge (b) spin wave modes measured at $\beta = 85°$, $H = 890$ Oe and several values of the bath temperature T_b. (c) Spin wave dispersion relation for BVSW and SSW modes of a 5 nm thick Py film at $H = 890$ Oe[65]. Arrows indicate energy- and momentum-conserving four-magnon scattering of two uniform mode magnons into two BVSW magnons with wave vectors k_4 and $-k_4$.

exclude the possibility that the observed microwave emission originates from magnetization oscillations localized within a small fraction of the nanowire's active region. This further corroborates the conclusion that SO torques excite spin wave eigenmodes of the system that occupy the entire length of the nanowire STO active region.

Measurements of the microwave signal emission as a function of temperature are also performed. Figs. 3.4a and 3.4b show the the dependence of the total integrated power in the bulk and edge groups of peaks measured at several values of the bath temperature T_b. The integrated power decreases with increasing T_b and vanishes at $T_b \approx 250$ K. The actual temperature of the nanowire is significantly higher than T_b due to Ohmic heating. The nanowire temperature can be estimated from measurements of the nanowire resistance as functions of T_b and I_{dc}[42] which is discussed in section 3.2.6. For $T_b = 4.2$ K, the actual nanowire temperature at I_c is approximately 150 K.

3.2.3 BLS measurements

In order to better understand the nature of the self-oscillatory dynamics induced by SO torques in the Pt/Py nanowire system and to directly confirm that the self-oscillatory modes occupy the entire active region of the nanowire, micro-focus Brillouin light scattering (BLS) measurements[66] of the current-driven magnetization dynamics in this system are performed. Since a 5 nm thick layer of Pt is not sufficiently transparent for BLS studies, a separate batch of samples was made for BLS measurements with the reverse order of deposition of the AlO_x, Py and Pt layers. These AlO_x(2 nm)Py(5 nm)/Pt(5-7 nm)/(sapphire substrate) nanowire samples are prepared by e-beam lithography and liftoff technique as described in section 3.4.1. The microwave signal emission from these samples is similar to that of the previous samples, with two notable differences: (i) the amplitude of self-oscillations of the edge mode is significantly higher than that of the bulk mode and (ii) the microwave emission from the edge mode persist up to room temperature. These differences are likely to originate from the different sample fabrication procedures: the lift-off fabrication process creates less nanowire edge damage than the Ar plasma etching process.

The main results of the BLS measurements are presented in Fig. 3.5. Fig. 3.5(a) shows a representative BLS spectrum measured by placing the probing laser spot at the center of the nanowire. In agreement with the results of electronic measurements of samples with Pt on top, the BLS spectrum exhibits a series of auto-oscillation peaks with the typical frequency separation of several hundred megahertz, which belong to the group of edge modes. By using the high spatial resolution of the BLS measurements, individual auto-oscillation peaks within the group are identified. For this the BLS detection frequency is fixed at the frequency of one of the peaks and spatial profiles of the dynamic magnetization are recorded by moving the probing laser spot along the nanowire axis with the spatial step size of 50 nm. As seen in Fig. 3.5(b), the spatial profiles corresponding to the two peaks are fundamentally different. While the profile for the first edge mode exhibits a slightly

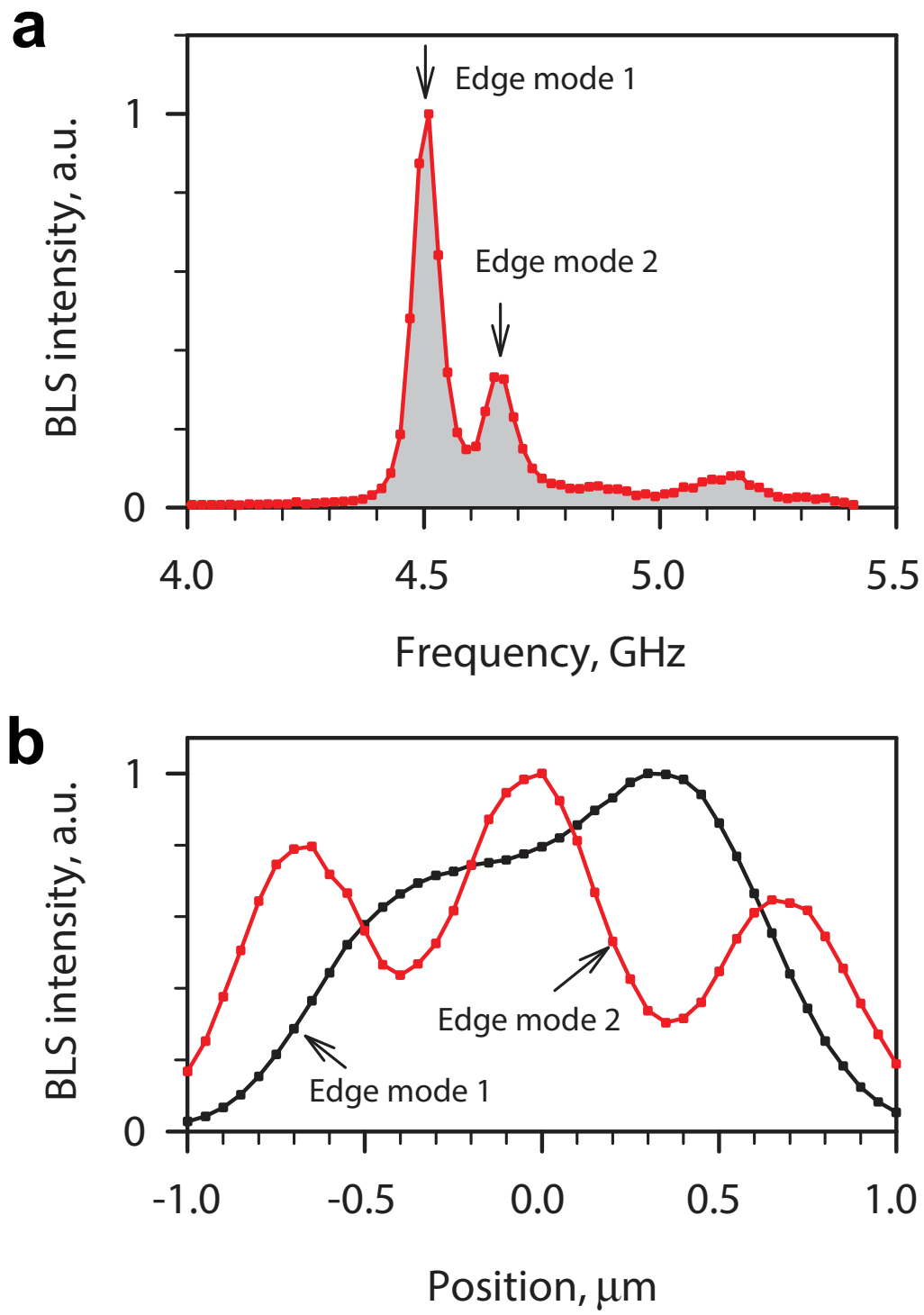

Figure 3.5: (a)BLS spectrum acquired by placing the probing laser spot at the center of the nanowire. BLS intensity is proportional to the intensity of the dynamic magnetization. (b)Spatial profiles of the intensity of the dynamic magnetization in the section parallel to the nanowire axis. The data were obtained at H=550 Oe and the bias current of 2.4 mA.

distorted bell-like shape, the profile for the second peak possesses three maxima. Based on the obtained data it is concluded that the individual auto-oscillation peaks within the groups correspond to the standing-wave modes quantized in the direction parallel to the nanowire axis[67]. The first peak corresponds to the combination of the fundamental mode having no nodes and the antisymmetric mode possessing one nodal line at the center. These two modes are indistinguishable in the spectrum, likely due to their small frequency separation. The second peak apparently corresponds to the mode possessing two nodal lines at the positions of the minima of the measured profile. It is important to note that since the BLS technique is sensitive to the intensity of the dynamic magnetization, the measured profile does not show a change of the sign across the positions of the nodal lines.

3.2.4 Material parameters of the Permalloy nanowire

Magnetic properties of the Py film in the Pt(5 nm)/Py(5 nm)/AlO_x(4 nm)/(GaAs substrate) nanowire samples are expected to differ from those of bulk Py. Previous studies of thin Py films interfaced with non-magnetic metallic layers and alumina have shown reduction of the saturation magnetization M_s[62] and presence of perpendicular surface anisotropy K_s[63,68]. In addition, patterning of the film into nanowires by Ar plasma etching creates material intermixing at the nanowire edges and results in magnetic edge dilution[61,64]. Therefore, in order to be able to predict the spectrum of spin wave eigenmodes of the nanowire, relevant magnetic parameters of the Py layer need to be extracted from experiment. This section expains how micromagnetic[23] fitting of three sets of experimental data: (i) wire resistance versus in-plane magnetic field, (ii) wire resistance versus out-of-plane magnetic field and (iii) quasi-uniform spin wave mode frequency versus magnetic field applied parallel to the wire axis is used to determine approximate values of saturation magnetization M_s, surface magnetic anisotropy K_s and the edge dilution depth D.

The value of the exchange stiffness of bulk Py $A \approx 10^{-6}$ erg/cm is known only approximately[69,70] due to the lack of reliable direct methods for measuring this quantity. It is also known that the value of A is usually reduced in thin films and nanomagnets compared to its bulk value[71]. In order to estimate the value of A for the Py layer in the nanowire device, the scaling relation $A \sim M_s^2$ and the value of saturation magnetization $M_s = 608$ emu/cm^3 extracted from the micromagnetic fit described below is used. This scaling predicts the exchange stiffness to be approximately half of the bulk value, and thus $A = 5 \times 10^{-7}$ erg/cm is adopted throughout all micromagnetic simulations in this chapter. Also, a thin-film value of the spectroscopic g-factor (g = 2.03) measured for a 5 nm thick Py film is employed[72]. For quantification of the magnetic edge dilution, the model developed in Ref. [61] is adopted, in which the saturation magnetization varies linearly from zero at the wire edge to the full film value M_s over the edge dilution depth D.

The micromagnetic fitting procedure begins by fitting the data of the normalized wire magnetoresistance $\hat{R}$ as a function of magnetic field H_{ip} applied in the plane of the sample perpendicular to the wire axis (Fig. 3.6 (a)). This is a convenient starting point because $\hat{R}(H_{ip})$ is independent of K_s, which directly establishes a relation between M_s and D through micromagnetic fitting to the $\hat{R}(H_{ip})$ data in Fig. 3.6 (a). The 190 nm wide, 5 nm thick Py nanowire is divided into 2 nm $\times$ 1 nm $\times$ 5 nm micromagnetic cells and the equilibrium configuration of magnetization for a given value of H_{ip} is found. Then the wire resistance R is calculated by dividing the wire onto $N = 190$ Py(5 nm)/Pt (5 nm) bilayer strips (each strip is 1 nm wide) along its length and use the equation for resistors connected in parallel to calculate the wire resistance $R = \left(\sum_{i=1}^{N} R_i^{-1}\right)^{-1}$. The resistance of each strip R_i $(i = 1..N)$ is calculated according to the AMR formula: $R_i = \tilde{R}_0 + \Delta\tilde{R}_i \cos^2(\theta_i)$, where $\tilde{R}_0 = NR_0$ is the resistance of the Py(5 nm)/Pt (5 nm) bilayer strip magnetized perpendicular to the strip axis, $\Delta\tilde{R}_i$ is the full AMR of the i-th strip, R_0 is the resistance of the nanowire magnetized perpendicular to the nanowire axis $\Delta R = \left(\sum_{i=1}^{N} \left(NR_0 + \Delta\tilde{R}_i\right)^{-1}\right)^{-1} - R_0$ is the full AMR of the nanowire and θ_i is the angle between magnetization in the i-th strip and the nanowire

axis. This equation for calculating the wire resistance is a good approximation because $\Delta R \ll R_0$ and the resistivities of Py and Pt are similar to each other. The simplifying assumption that $\Delta\tilde{R}_i$ in the i-th strip is proportional to the value of M_s in this strip[15] is made so that AMR is reduced at the nanowire edges due to the magnetic dilution.

Several values of the edge dilution depth D is chosen between 0 and 70 nm, and for each value of D a set of micromagnetic simulations is performed to determine the value of M_s that gives the best fit to the $\hat{R}(H_{ip})$ data. The resulting dependence of M_s on D is shown by circles in Fig. 3.6 (b). A fourth order polynomial fit to the data is performed and shown in Fig. 3.6 (b) which thereby establishes the functional dependence $M_s(D)$ that is used throughout the rest of the micromagnetic simulations.

The fit of the normalized nanowire magnetoresistance data measured as a function of magnetic field H_{op} applied perpendicular to the sample plane is shown in Fig. 3.7(a). A set of micromagnetic simulations is performed for several values of the edge dilution depth D between 0 and 70 nm, and for each value of D, the value of K_s is found that gave the best micromagnetic fit to the $\hat{R}(H_{op})$ data in Fig. 3.7(a). In these simulations, the function $M_s(D)$ established in the $\hat{R}(H_{ip})$ fitting is used. The resulting dependence of K_s on D is shown by circles in Fig. 3.7(b). Fitting a fourth order polynomial to the data in Fig. 3.7(b) gives the functional relation $K_s(D)$ that is used throughout the rest of the micromagnetic simulations.

In order to determine the value of D that best describes the properties of the nanowire device, measurements of the quasi-uniform spin wave mode frequency f_q as a function of magnetic field $H_{||}$ applied parallel to the nanowire axis is used. These measurements are made by the spin torque ferromagnetic resonance (ST-FMR) technique[24,25] described in section 3.2.2. The measured dependence of f_q on $H_{||}$ is shown by crosses in Fig. 3.8. To find the theoretical dependence $f_q(H_{||})$, micromagnetic simulations is employed to calculate the spectrum of spin wave eigenmodes of the nanowire. For these simulations, a pulse of SO torque and a pulse

of Oersted field is simultaneously applied to the nanowire magnetization. Both pulses are generated by a spatially uniform sinc-shaped current pulse applied to the nanowire[73]:

$$I(t) = I_0 \frac{\sin(2\pi f_c t)}{2\pi f_c t} \tag{3.1}$$

Such a current pulse excites all spin wave eigenmodes of the system that have amplitude profiles symmetric with respect to the nanowire center and have frequencies below the cutoff frequency $f_c = 20$ GHz. The current pulse amplitude is chosen to be small enough that the magnetization dynamics remains in the linear regime. The magnetization of each micromagnetic cell is recorded as a function of time and then Fourier transformed. Peaks in the Fourier transform amplitude of the dynamic magnetization correspond to frequencies of spin wave eigenmodes of the nanowire. For a magnetic field $H_{||}$ applied along the length of the nanowire, the simulations show that the lowest frequency mode is the quasi-uniform spin wave mode without nodes along the wire width. The simulations show that the frequency of this mode depends on the edge dilution depth D and therefore can be used with the experimental data in Fig. 3.8 to determine the value of D appropriate for the nanowire device. Using the functions $M_s(D)$ and $K_s(D)$ established by the magnetoresistance data fitting, a single parameter (D) fit of the data in Fig. 3.8 is performed and the best agreement with the data for $D = 10$ nm is found. The solid line in Fig. 3.8 shows the best fit to the data for $D = 10$ nm.

The micromagnetic fitting described above gives the set of magnetic parameters accurately describing the magnetic properties of the nanowire device: $D = 10$ nm, $M_s(10\text{ nm}) = 608$ emu/cm^3 and $K_s(10\text{ nm}) = 0.237$ erg/cm^2. Using these parameters, micromagnetic simulations are performed to determine the spectrum of the nanowire spin wave eigenmodes for magnetic field applied in the plane of the sample at the angle $\beta = 85^\circ$ with respect to the nanowire axis. As in the easy-axis field case described above, a pulse of SO torque and Oersted field generated by a spatially uniform sinc-shaped current pulse is applied and

the spin wave eigenmode frequencies is determined from the positions of spectral peaks in the Fourier transform of the time-dependent dynamic magnetization. The lowest frequency mode is found to be the edge eigenmode, whose amplitude is maximum at the wire edge. Its spatial profile across the wire width is shown in the inset of Fig. 3.2. The next lowest frequency mode has bulk character and exhibits maximum amplitude in the center of the wire as shown in the inset of Fig. 3.2. Solid lines in Fig. 3.3 show the calculated dependence of frequencies of these two modes on the applied magnetic field.

3.2.5 Precession Cone Angle Estimate

In this section, the precession cone angle θ_b achieved by the bulk mode in the self-oscillatory regime is estimated based on comparison of the measured integrated power P_b in the bulk group of microwave emission peaks to the integrated power predicted to arise from self-oscillations of the bulk mode with the amplitude θ_b in an ideal nanowire. The bulk mode profile across the nanowire width for an ideal nanowire is calculated micromagnetically as described in the previous section and is shown in the inset of Fig. 3.2(a).

The measured integrated power at the fundamental frequency emitted by the bulk group of modes P_b (corrected for frequency-dependent attenuation and amplification in the measurement circuit) is plotted as a function of direct bias current I_{dc} inFig. 3.3(c). This power is directly related to the amplitude of the nanowire resistance oscillations δR_{ac1} at the fundamental frequency of magnetization self-oscillations. The microwave voltage generated by the nanowire STO device at the fundamental frequency of the bulk mode $I_{dc}\delta R_{ac1}$ is detected by a 50 Ohm microwave spectrum analyzer as microwave power P_b[26]:

$$P_b = \frac{1}{2R_{50}} \left(I_{dc}\delta R_{ac1} \frac{R_{50}}{R + R_{50}} \right)^2 \tag{3.2}$$

where $R_{50} \equiv 50$ Ohm is the spectrum analyzer impedance and R is the nanowire resistance. From this equation, the amplitude of resistance oscillations at the fundamental frequency as a function of the emitted power is expressed as:

$$\delta R_{ac1} = \frac{R + R_{50}}{I_{dc}\sqrt{R_{50}}}\sqrt{2P_b} \tag{3.3}$$

On the other hand, δR_{ac} for a given value of θ_b can be calculated from the micromagnetic bulk mode profile shown in the inset of Fig. 3.2(a). For this calculation, the wire is divided into $N = 190$ strips along its length and an approximate time dependence of the in-plane angle $\theta_i(t)$ of magnetization is calculated with respect to the nanowire axis in the i-th strip according to the following equation:

$$\theta_i(t) = \theta_{i0} + a_i\theta_b \sin(\omega t + \varphi_i) \tag{3.4}$$

In this expression, θ_{i0} is the equilibrium direction of magnetization in the i-th strip, a_i is the normalized bulk mode profile shown in the inset of Fig. 3.2(a) ($a_i = 1$ in the wire center), ω is the bulk mode angular eigenfrequency, φ_i is the phase of the bulk mode in the i-th strip and θ_b is the precession cone angle of the bulk mode (defined as the precession cone angle in the center of the nanowire).

Next, the AMR formula is employed to calculate the time dependence of resistance $R_i(t)$ of the i-th strip:

$$R_i(t, \theta_b) = \tilde{R}_0 + \Delta\tilde{R}_i \cos^2(\theta_i(t)) \tag{3.5}$$

Finally, the time dependent resistance of the nanowire is calculated as:

$$R(t, \theta_b) = \left(\sum_{i=1}^{N} \frac{1}{R_i(t, \theta_b)}\right)^{-1} \tag{3.6}$$

This expression is then expanded into a Fourier series to find the amplitudes of resistance oscillations at the fundamental frequency δR_{ac1} and the second harmonic δR_{ac2}. Fig. 3.9 shows the calculated δR_{ac1} and δR_{ac2} as functions of the precession cone angle θ_b. The horizontal dashed line in this figure marks the the value of δR_{ac1} determined via Eq. 3.3 from the experimentally measured integrated power $P_b = 9.0$ pW at $I_{dc} = 2.4125$ mA and $H = 890$ Oe applied at angle $\beta = 85^\circ$ with respect to the nanowire axis. The intersection of this line with the theoretical curve $\delta R_{ac1}(\theta_b)$ gives an estimate of the precession cone angle $\theta_b \approx 18.4^\circ$ at these current and field values. The horizontal dotted line in this figure is δR_{ac2} evaluated via Eq. 3.3 from the measured integrated power in the second harmonic $P_{b2} = 15.5$ pW for the same current and field bias values. The intersection of this line with the theoretically calculated $\delta R_{ac2}(\theta_b)$ gives an independent estimate of the precession cone angle $\theta_b = 24.3^\circ$. The few degree difference between these two estimates of θ_b most probably arises from simplifications of the theoretical model assuming perfect nanowire with translational invariance along the wire axis. Nevertheless, these two independent estimates show that precession cone angles can reach values of tens of degrees in the regime of self-oscillations.

3.2.6 Sample Temperature

Direct current bias I_{dc} can significantly increase the temperature of the nanowire due to Ohmic heating. In order to estimate the actual temperature of the nanowire at large I_{dc}, measurements of the wire resistance as a function of temperature at small $I_{dc} = 0.1$ mA to measurements of the wire resistance versus I_{dc} taken at the bath temperature $T_b = 4.2$ K is compared[42]. This data is plotted in Fig. 3.10, which shows that resistance of the nanowire is approximately quadratic in both T_b and I_{dc}. This allows for an estimate of the actual temperature of the nanowire directly from Fig. 3.10. For example, at $I_{dc} = 2.0$ mA, the actual temperature of the nanowire $T \approx 150$ K.

3.2.7 Critical Current Density Estimate

In this section, the expected critical current density for excitation of self-oscillations of magnetization in the Pt/Py bilayer nanowire is estimated and compared to the experimentally measured critical current density. The critical spin current density injected from the Pt layer into the Py layer J_S (measured in units of charge current density) is given by[55]:

$$J_S = \frac{2e}{\hbar}\alpha \left(H_{eff} + 2\pi M_{eff}\right) M_s t \tag{3.7}$$

where $H_{eff} \approx 600$ Oe is the in-plane effective field approximately equal to the hard-axis applied field minus the in-plane hard-axis saturation field, $M_{eff} = M_s - K_s/(2\pi M_s t) = 484$ emu/cm^3, $t = 5$ nm is the Py layer thickness, and $\alpha = 0.023$ is the Gilbert damping constant appropriate for a 5 nm thick Py layer interfaced on one side with a Pt layer[74]. Eq. (3.7) gives the expected critical spin current density $J_S = 7.7 \times 10^6$ A/cm^2. This value should be compared to the measured critical spin current density in the Pt/Py bilayer nanowire system. Using the thin-film resistivity values of Pt and Py layers (ρ_{Pt} =20 $\mu\Omega$ cm and ρ_{Py} =45 $\mu\Omega$ cm[55]) and taking into account that the critical charge current for excitation of magnetization self oscillations in the bilayer nanowire is approximately 2.2 mA, the critical charge current density in the Pt layer is calculated to be $J_C = 1.6 \times 10^8$ A/cm^2. The corresponding transverse critical spin current density can be estimated as $J_S \approx \theta_{SH} J_C$[55], where θ_{SH} is the spin Hall angle in Pt. Assuming $\theta_{SH} = 0.056$[55], the estimated critical spin current density is $J_S = 9.0 \times 10^6$ A/cm^2, which is similar to the value expected for this system.

It is also instructive to compare the estimated critical spin current density in the Pt/Py bilayer system to that measured in Py(5.5 nm)/Cu(20 nm)/Py(20 nm) spin valve nanopillars[75]. The critical charge current density measured in these nanopillar devices is $J_C = 1.75 \times 10^7$ A/cm^2. Assuming spin current polarization $P = 0.3$, the measured critical spin current

density is $J_S = P \cdot J_C = 5.2 \times 10^6$ A/cm^2. This value is nearly one half of the critical spin current density measured for the Pt/Py nanowire system, which is consistent with the damping of the Py free layer in the nanopillar ($\alpha = 0.01$[75]) being approximately half of that in the Pt/Py system.

3.3 Discussion

Recent experiments[54] demonstrated that application of spatially uniform SO torques to an extended ferromagnetic film does not result in excitation of magnetic self-oscillations because the amplitudes of all spin wave modes of the film are limited by nonlinear magnon scattering processes. Therefore, this observation of self-oscillatory dynamics excited by SO torques in the entire 1.8 μm long active region of a ferromagnetic nanowire is surprising. Thi suggests that the quantization of the spin wave spectrum in the nanowire geometry reduces the number of available nonlinear magnon scattering channels and thereby enables excitation of self-oscillatory dynamics of the low-energy spin wave eigenmodes of the nanowire.

Fig. 3.4(c) shows the spin wave dispersion relation of a 5 nm thick Py film calculated for spin wave propagating parallel (backward volume spin waves, BVSW) and perpendicular (surface spin waves, SSW) to the in-plane magnetization vector[65]. Energy- and momentum-conserving four-magnon scattering processes from the uniform ($\mathbf{k} = 0$) mode into spin wave modes with a finite wave vector $\mathbf{k}_4$ are allowed for the BVSW but not for the SSW modes as schematically illustrated in Fig. 3.4(c). This nonlinear scattering channel is always present in the 2D film geometry and it contributes to the nonlinear damping of the uniform mode. When such a film is patterned into a nanowire aligned perpendicular to the magnetization direction, the BVSW mode spectrum becomes quantized and the energy-conserving four-magnon scattering channel becomes suppressed for a wire of width $w < \pi k_4^{-1}$. This example illustrates how a nonlinear scattering channel present in the 2D film geometry becomes

suppressed in the 1D nanowire geometry. A number of other higher-order nonlinear scattering channels allowed by symmetry in the film are also suppressed in the nanowire due to breaking of translational invariance in the direction perpendicular to the nanowire axis.

Since multiple nonlinear magnon scattering processes responsible for limiting the amplitude of low-frequency spin wave modes are eliminated in the nanowire, ST excitation of large-amplitude self-oscillatory spin wave modes may become possible above the critical current. At higher currents, SO torques increase the occupation numbers for all magnon modes, which results in (i) enhanced scattering in the remaining nonlinear channels and the associated decrease of the amplitude of self-oscillations seen in Fig. 3.3(c) and (ii) reduction of the saturation magnetization and the associated decrease of the self-oscillatory mode frequency with current seen in Fig. 3.2(c). The data in Fig. 3.4 showing decreasing self-oscillation amplitude with increasing temperature suggest that magnon-phonon scattering might also play a role in suppression of the self-oscillatory dynamics. Development of a detailed theory accounting for all magnon scattering channels in the nanowire in the presence of SO torques is required for quantitative explanation of the experimental data, and hopefully this work will stimulate the development of such a theory.

In conclusion, this chapter demonstrated that spatially uniform spin torques can excite self-oscillations of magnetization in a 1D ferromagnetic system – a Pt/Py bilayer nanowire. The self-oscillatory modes induced by spin torque in this system directly arise from the bulk and edge spin wave eigenmodes of the nanowire. The 1D nanowire geometry offers unique advantages for studies of magnetization dynamics driven by spin torques over the 2D extended thin film system, in which spatially uniform spin torque does not excite magnetization self-oscillations. This result suggests that the self-oscillatory dynamics in the nanowire geometry is enabled by geometric confinement of magnons that suppresses a number of nonlinear magnon scattering channels. This chapter demonstrates the feasibility of spin torque oscillators with the active region dimensions extended beyond the nanometer length scale.

3.4 Methods

3.4.1 Sample fabrication

All layers of the Pt(5 nm)/Py(5 nm)/AlO_x(4 nm)/(GaAs substrate) samples are deposited by magnetron sputtering at room temperature. The 6 μm long nanowires are defined via e-beam lithography and Ar plasma etching using e-beam evaporated Cr mask. The Au(35 nm)/Cr(7 nm) leads with a 1.8 μm gap between them defining the active region of the nanowire STO are made via e-beam lithography and e-beam evaporation of the Au/Cr bilayer followed lift-off. The fabrication process of the AlOx(2 nm)Py(5 nm)/Pt(5-7 nm)/(sapphire substrate) samples for the micro-BLS measurements starts with deposition of a 5 nm thick Pt layer onto a sapphire substrate at 550 °C, which results in growth of a continuous Pt film as verified by high resolution SEM and atomic force microscopy imaging. Then the nanowire is defined on top of the Pt film via e-beam lithography, brief Ar plasma cleaning immediately followed by *in situ* room temperature sputter deposition of a AlOx(3 nm)/Py(5 nm)/Pt(2 nm) trilayer, and lift-off. The Au(40 nm)/Cr(7 nm) leads are defined via e-beam lithography and e-beam evaporation of the Au/Cr bilayer followed by lift-off. As the final fabrication step, Ar plasma etching is used to remove the 5 nm thick bottom Pt layer everywhere but under the Py nanowire and the Au/Cr leads.

3.4.2 BLS measurements.

Micro-focus BLS measurements were performed at room temperature by focusing light produced by a continuous-wave single-frequency laser operating at a wavelength of 532 nm into a diffraction-limited spot. The light scattered from magnetic oscillations was analyzed by a six-pass Fabry-Perot interferometer TFP-1 (JRS Scientific Instruments, Switzerland) to

obtain information about the BLS intensity proportional to the square of the amplitude of the dynamic magnetization at the location of the probing spot.

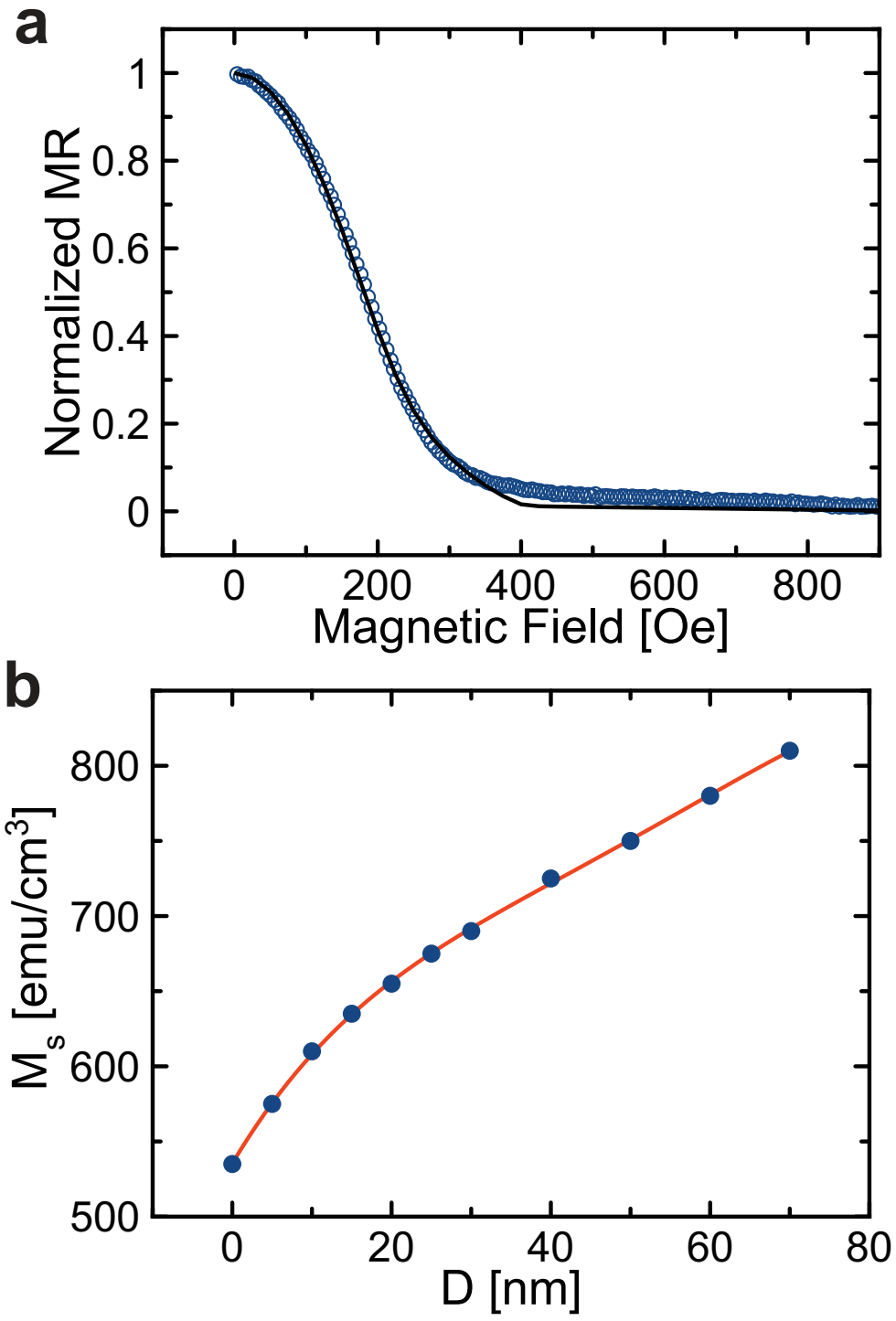

Figure 3.6: (a) Normalized magnetoresistance of a 190-nm wide Pt(5 nm)/Py(5 nm) nanowire measured as a function of magnetic field applied in the plane of the sample perpendicular to the nanowire axis (circles). The solid line shows a micromagnetic fit to the data for the edge dilution depth $D = 10$ nm, which gives the value of $M_s = 608$ emu/cm^3. (b) Circles show the dependence of M_s on D given by the micromagnetic fit to the data in (a). The line is a fourth order polynomial fit to the data.

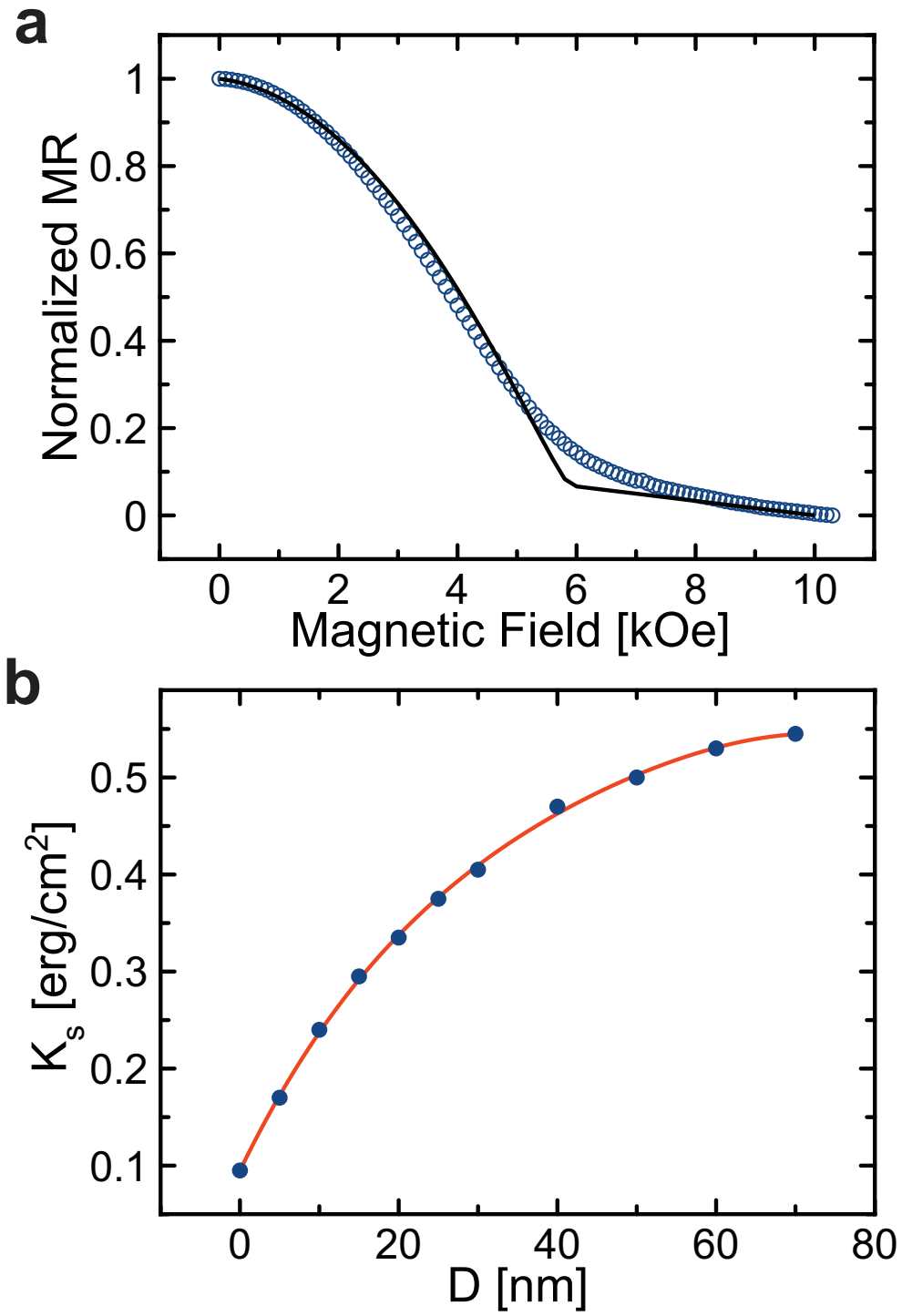

Figure 3.7: (a) Normalized magnetoresistance of a 190-nm wide Pt(5 nm)/Py(5 nm) nanowire measured as a function of the magnetic field applied normal to the sample plane (circles). The line shows the micromagnetic fit to the data for the edge dilution depth $D =$ 10 nm, which gives the value of $K_s = 0.237$ erg/cm^2. (b) Circles show the dependence of K_s on D given by the micromagnetic fitting to the data in (a). The line is a fourth order polynomial fit to the data.

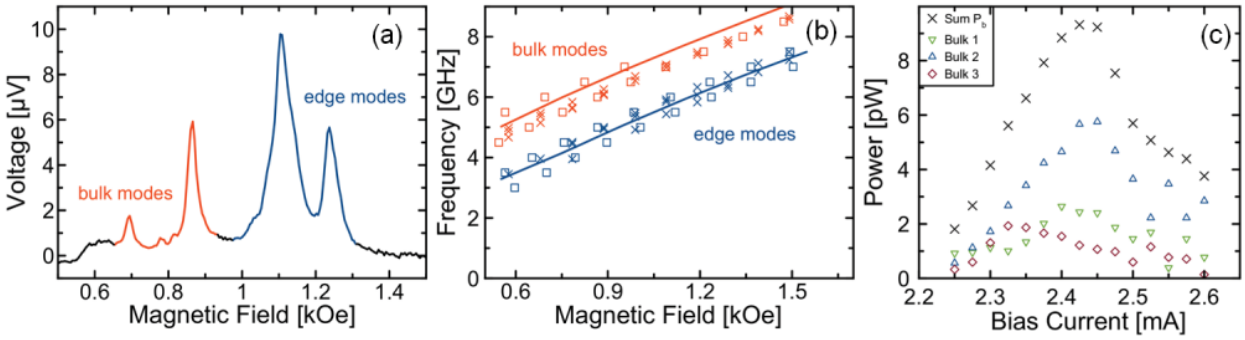

Figure 3.8: Frequency f_q of the quasi-uniform spin wave mode of the nanowire as a function of magnetic field $H_{||}$ applied parallel to the nanowire axis. Crosses show the experimental data measured by ST-FMR, the line is the micromagnetic calculation result for the edge dilution depth $D = 10$ nm.

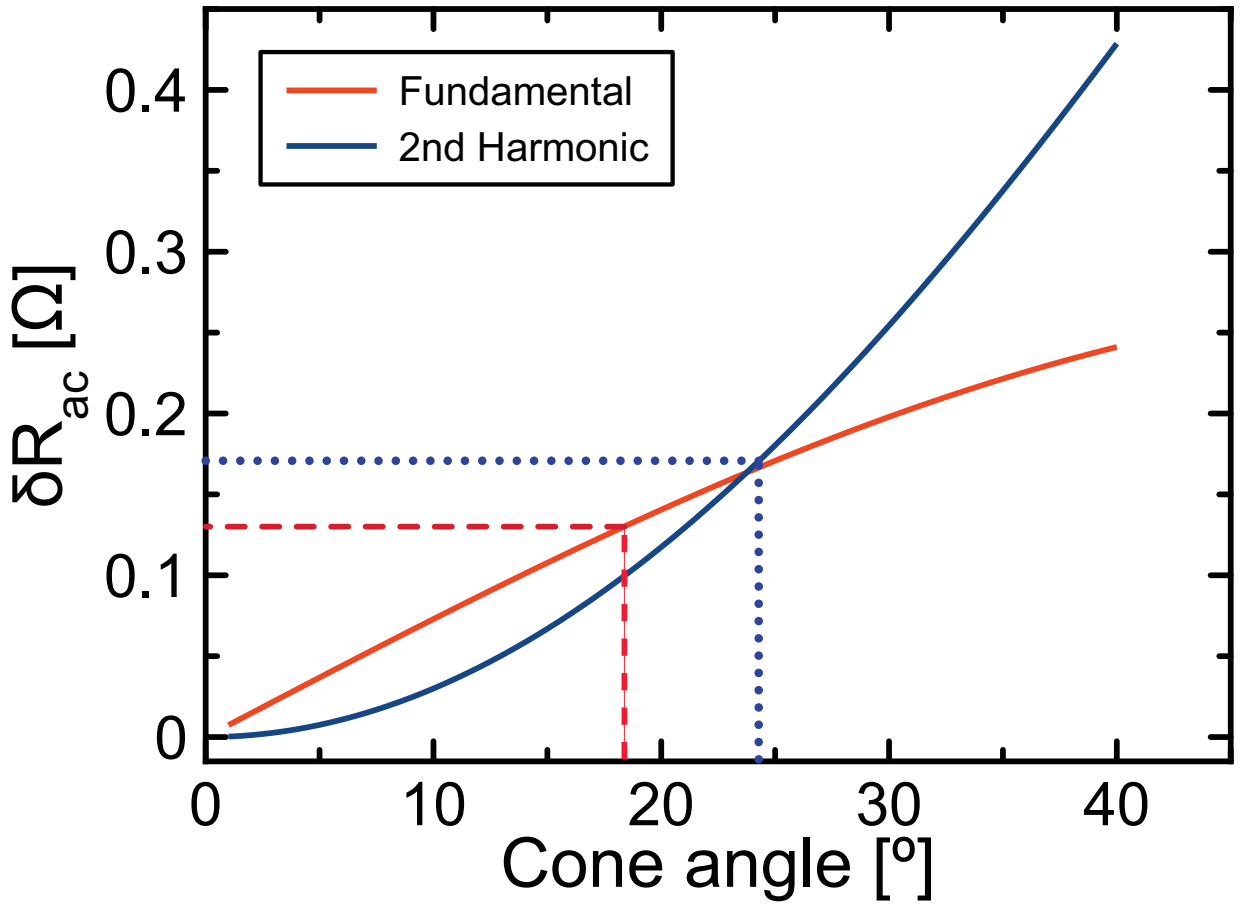

Figure 3.9: Dependence of the amplitude of resistance oscillations at the fundamental frequency δR_{ac1} and the second harmonic δR_{ac2} of the bulk mode on the precession cone angle θ_b. The solid lines are theoretical curves based on micromagnetic simulations of the bulk mode profile. The horizontal dashed and dotted lines mark the amplitude of resistance oscillations at the fundamental frequency and the second harmonic determined from the measured values (at $I_{dc} = 2.4125$ mA) of the integrated power in the fundamental ($P_b = 9.0$ pW) and second harmonic ($P_{b2} = 15.5$ pW) of the bulk group of peaks.

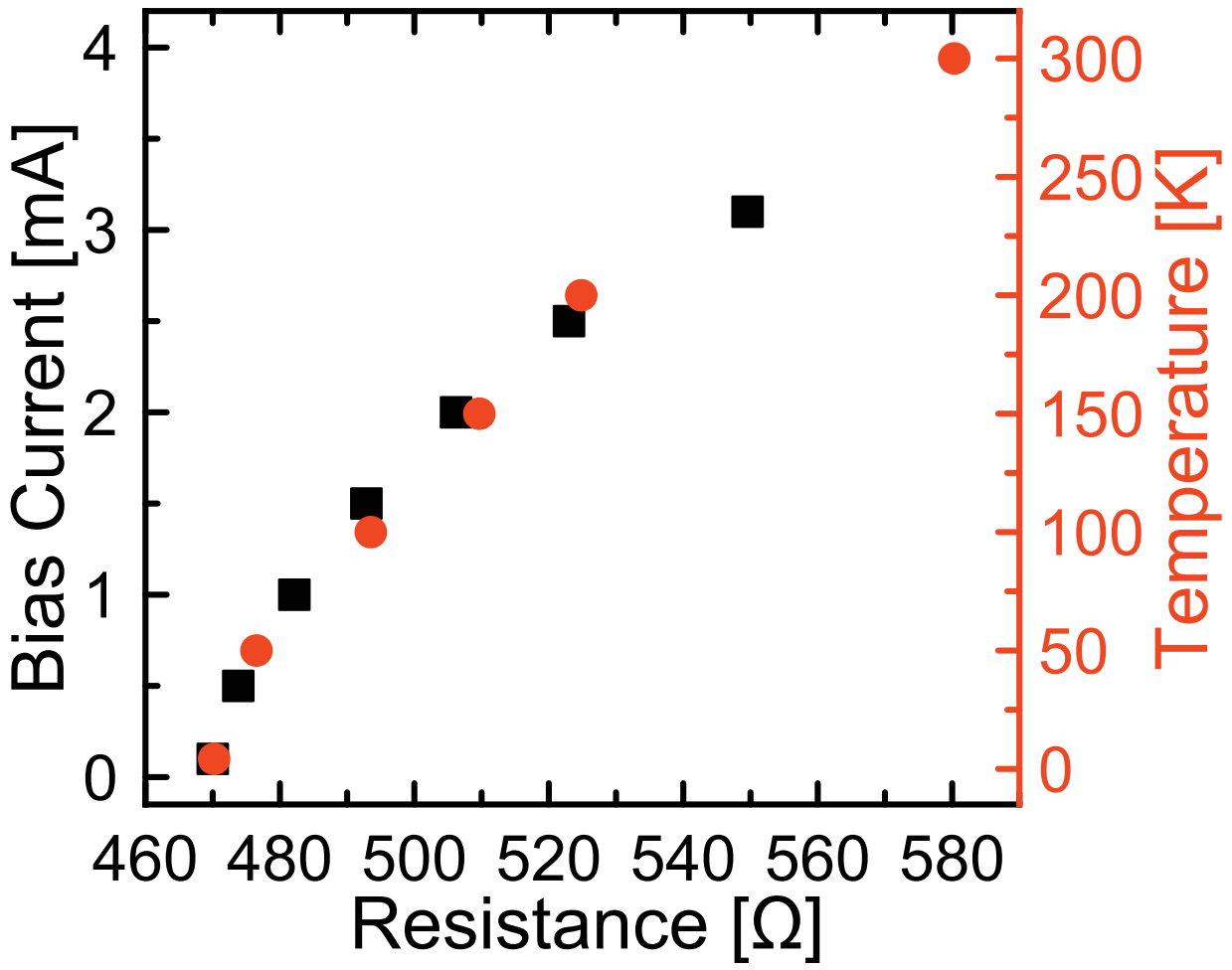

Figure 3.10: Resistance of the nanowire measured as a function of temperature at direct bias current $I_{dc} = 0.1$ mA (circles) and as a function of I_{dc} at the bath temperature $T_b = 4.2$ K (squares).

Bibliography

[1] J.C. Slonczewski. "Current-driven excitation of magnetic multilayers". In: *Journal of Magnetism and Magnetic Materials* 159.1-2 (1996), pp. L1–L7. DOI: doi:10.1016/0304-8853(96)00062-5. URL: http://dx.doi.org/10.1016/0304-8853(96)00062-5.

[2] L. Berger. "Emission of spin waves by a magnetic multilayer traversed by a current". In: *Phys. Rev. B* 54.13 (1996), pp. 9353–9358. DOI: http://dx.doi.org/10.1103/PhysRevB.54.9353. URL: http://dx.doi.org/10.1103/PhysRevB.54.9353.

[5] D'yakonov M.I. and Perel' V. I. "Possibility of Orienting Electron Spins with Current". In: *Sov. Phys. JETP Lett.* 13.11 (1971), p. 467. URL: http://www.jetpletters.ac.ru/ps/1587/article_24366.pdf.

[6] J. E. Hirsch. "Spin Hall Effect". In: *Phys. Rev. Lett.* 83.9 (1999), pp. 1834–1837. DOI: http://dx.doi.org/10.1103/PhysRevLett.83.1834. URL: http://dx.doi.org/10.1103/PhysRevLett.83.1834.

[11] Axel Hoffmann. "Spin Hall Effects in Metals". In: *IEEE Trans. Magn.* 49.10 (2013), pp. 5172–5193. DOI: 10.1109/TMAG.2013.2262947. URL: http://dx.doi.org/10.1109/TMAG.2013.2262947.

[15] T. McGuire and R. Potter. "Anisotropic magnetoresistance in ferromagnetic 3d alloys". In: *IEEE Trans. Magn.* 11.4 (1975), pp. 1018–1038. DOI: 10.1109/TMAG.1975.1058782. URL: http://dx.doi.org/10.1109/TMAG.1975.1058782.

[23] M.J. Donahue and D.G. Porter. *OOMMF User's Guide, Version 1.0*. Interagency Report NISTIR 6376. Gaithersburg, MD: National Institute of Standards and Technology, 1999.

[24] A. A. Tulapurkar et al. "Spin-torque diode effect in magnetic tunnel junctions". In: *Nature* 438.7066 (2005), pp. 339–342. DOI: 10.1038/nature04207. URL: http://dx.doi.org/10.1038/nature04207.

[25] J. C. Sankey et al. "Spin-Transfer-Driven Ferromagnetic Resonance of Individual Nanomagnets". In: *Phys. Rev. Lett.* 96.22 (2006). DOI: http://dx.doi.org/10.1103/PhysRevLett.96.227601. URL: http://dx.doi.org/10.1103/PhysRevLett.96.227601.

[26] S. I. Kiselev et al. "Microwave oscillations of a nanomagnet driven by a spin-polarized current". In: *Nature* 425.6956 (2003), pp. 380–383. DOI: 10.1038/nature01967. URL: http://dx.doi.org/10.1038/nature01967.

[27] Zheng Duan et al. "Nanowire spin torque oscillator driven by spin orbit torques". In: *Nature Communications* 5 (2014), p. 5616. DOI: doi:10.1038/ncomms6616. URL: http://dx.doi.org/10.1038/ncomms6616.

[28] A. Slavin and V. Tiberkevich. "Nonlinear Auto-Oscillator Theory of Microwave Generation by Spin-Polarized Current". In: *IEEE Trans. Magn.* 45.4 (2009), pp. 1875–1918. DOI: 10.1109/TMAG.2008.2009935. URL: http://dx.doi.org/10.1109/TMAG.2008.2009935.

[29] B. zyilmaz et al. "Current-Induced Excitations in Single Cobalt Ferromagnetic Layer Nanopillars". In: *Phys. Rev. Lett.* 93.17 (2004). DOI: http://dx.doi.org/10.1103/PhysRevLett.93.176604. URL: http://dx.doi.org/10.1103/PhysRevLett.93.176604.

[30] Q. Mistral et al. "Current-driven microwave oscillations in current perpendicular-to-plane spin-valve nanopillars". In: *Appl. Phys. Lett.* 88.19 (2006), p. 192507. DOI: http://dx.doi.org/10.1063/1.2201897. URL: http://dx.doi.org/10.1063/1.2201897.

[31] P M Braganca et al. "Nanoscale magnetic field detection using a spin torque oscillator". In: *Nanotechnology* 21.23 (2010), p. 235202. DOI: 10.1088/0957-4484/21/23/235202. URL: http://dx.doi.org/10.1088/0957-4484/21/23/235202.

[32] W. Rippard et al. "Direct-Current Induced Dynamics in C o 90 F e 10 / N i 80 F e 20 Point Contacts". In: *Phys. Rev. Lett.* 92.2 (2004). DOI: 10.1103/PhysRevLett.92.027201. URL: http://dx.doi.org/10.1103/PhysRevLett.92.027201.

[33] A. Ruotolo et al. "Phase-locking of magnetic vortices mediated by antivortices". In: *Nature Nanotech* 4.8 (2009), pp. 528–532. DOI: 10.1038/nnano.2009.143. URL: http://dx.doi.org/10.1038/nnano.2009.143.

[34] S. M. Mohseni et al. "Spin Torque-Generated Magnetic Droplet Solitons". In: *Science* 339.6125 (2013), pp. 1295–1298. DOI: 10.1126/science.1230155. URL: http://dx.doi.org/10.1126/science.1230155.

[35] Alexey V. Nazarov et al. "Spin transfer stimulated microwave emission in MgO magnetic tunnel junctions". In: *Appl. Phys. Lett.* 88.16 (2006), p. 162504. DOI: http://dx.doi.org/10.1063/1.2196232. URL: http://dx.doi.org/10.1063/1.2196232.

[36] Alina M. Deac et al. "Bias-driven high-power microwave emission from MgO-based tunnel magnetoresistance devices". In: *Nat Phys* 4.10 (2008), pp. 803–809. DOI: 10.1038/nphys1036. URL: http://dx.doi.org/10.1038/nphys1036.

[37] D. Houssameddine et al. "Spin transfer induced coherent microwave emission with large power from nanoscale MgO tunnel junctions". In: *Appl. Phys. Lett.* 93.2 (2008), p. 022505. DOI: http://dx.doi.org/10.1063/1.2956418. URL: http://dx.doi.org/10.1063/1.2956418.

[38] B. Georges et al. “Origin of the spectral linewidth in nonlinear spin-transfer oscillators based on MgO tunnel junctions”. In: *Phys. Rev. B* 80.6 (2009). DOI: http://dx.doi.org/10.1103/PhysRevB.80.060404. URL: http://dx.doi.org/10.1103/PhysRevB.80.060404.

[39] Graham E. Rowlands et al. “Time Domain Mapping of Spin Torque Oscillator Effective Energy”. In: *Phys. Rev. Lett.* 111.8 (2013). DOI: http://dx.doi.org/10.1103/PhysRevLett.111.087206. URL: http://dx.doi.org/10.1103/PhysRevLett.111.087206.

[40] Vladislav E. Demidov et al. “Magnetic nano-oscillator driven by pure spin current”. In: *Nature Materials* (2012). DOI: 10.1038/nmat3459. URL: http://dx.doi.org/10.1038/nmat3459.

[41] Luqiao Liu et al. “Magnetic Oscillations Driven by the Spin Hall Effect in 3-Terminal Magnetic Tunnel Junction Devices”. In: *Phys. Rev. Lett.* 109.18 (2012). DOI: http://dx.doi.org/10.1103/PhysRevLett.109.186602. URL: http://dx.doi.org/10.1103/PhysRevLett.109.186602.

[42] R. H. Liu, W. L. Lim, and S. Urazhdin. “Spectral Characteristics of the Microwave Emission by the Spin Hall Nano-Oscillator”. In: *Phys. Rev. Lett.* 110.14 (2013). DOI: http://dx.doi.org/10.1103/PhysRevLett.110.147601. URL: http://dx.doi.org/10.1103/PhysRevLett.110.147601.

[43] Paul M. Haney et al. “Current induced torques and interfacial spin-orbit coupling: Semiclassical modeling”. In: *Phys. Rev. B* 87.17 (2013). DOI: http://dx.doi.org/10.1103/PhysRevB.87.174411. URL: http://dx.doi.org/10.1103/PhysRevB.87.174411.

[44] Junyeon Kim et al. “Layer thickness dependence of the current-induced effective field vector in Ta|CoFeB|MgO”. In: *Nature Materials* 12.3 (2012), pp. 240–245. DOI: 10.1038/nmat3522. URL: http://dx.doi.org/10.1038/nmat3522.

[45] Eduardo Martinez, Satoru Emori, and Geoffrey S. D. Beach. “Current-driven domain wall motion along high perpendicular anisotropy multilayers: The role of the Rashba field, the spin Hall effect, and the Dzyaloshinskii-Moriya interaction”. In: *Appl. Phys. Lett.* 103.7 (2013), p. 072406. DOI: http://dx.doi.org/10.1063/1.4818723. URL: http://dx.doi.org/10.1063/1.4818723.

[46] Shufeng Zhang. “Spin Hall Effect in the Presence of Spin Diffusion”. In: *Phys. Rev. Lett.* 85.2 (2000), pp. 393–396. DOI: http://dx.doi.org/10.1103/PhysRevLett.85.393. URL: http://dx.doi.org/10.1103/PhysRevLett.85.393.

[47] K. Ando et al. “Electric Manipulation of Spin Relaxation Using the Spin Hall Effect”. In: *Phys. Rev. Lett.* 101.3 (2008). DOI: http://dx.doi.org/10.1103/PhysRevLett.101.036601. URL: http://dx.doi.org/10.1103/PhysRevLett.101.036601.

[48] Xin Fan et al. “Observation of the nonlocal spin-orbital effective field”. In: *Nature Communications* 4 (2013), p. 1799. DOI: 10.1038/ncomms2709. URL: http://dx.doi.org/10.1038/ncomms2709.

[49] Lihui Bai et al. "Universal Method for Separating Spin Pumping from Spin Rectification Voltage of Ferromagnetic Resonance". In: *Phys. Rev. Lett.* 111.21 (2013). DOI: http://dx.doi.org/10.1103/PhysRevLett.111.217602. URL: http://dx.doi.org/10.1103/PhysRevLett.111.217602.

[50] Rashba E. I. Bychkov Yu. A. "Properties of a 2D electron gas with lifted spectral degeneracy". In: *JETP Lett.* 39 (1984), p. 66. URL: http://www.jetpletters.ac.ru/ps/1264/article_19121.shtml.

[51] Jairo Sinova et al. "Universal Intrinsic Spin Hall Effect". In: *Phys. Rev. Lett.* 92.12 (2004). DOI: http://dx.doi.org/10.1103/PhysRevLett.92.126603. URL: http://dx.doi.org/10.1103/PhysRevLett.92.126603.

[52] Katsunori Obata and Gen Tatara. "Current-induced domain wall motion in Rashba spin-orbit system". In: *Phys. Rev. B* 77.21 (2008). DOI: 10.1103/PhysRevB.77.214429. URL: http://dx.doi.org/10.1103/PhysRevB.77.214429.

[53] Ioan Mihai Miron et al. "Current-driven spin torque induced by the Rashba effect in a ferromagnetic metal layer". In: *Nature Materials* (2010). DOI: 10.1038/nmat2613. URL: http://dx.doi.org/10.1038/nmat2613.

[54] V. E. Demidov et al. "Control of Magnetic Fluctuations by Spin Current". In: *Phys. Rev. Lett.* 107.10 (2011). DOI: http://dx.doi.org/10.1103/PhysRevLett.107.107204. URL: http://dx.doi.org/10.1103/PhysRevLett.107.107204.

[55] Luqiao Liu et al. "Spin-Torque Ferromagnetic Resonance Induced by the Spin Hall Effect". In: *Phys. Rev. Lett.* 106.3 (2011). DOI: http://dx.doi.org/10.1103/PhysRevLett.106.036601. URL: http://dx.doi.org/10.1103/PhysRevLett.106.036601.

[56] C. Wang et al. "Bias and angular dependence of spin-transfer torque in magnetic tunnel junctions". In: *Phys. Rev. B* 79.22 (2009). DOI: http://dx.doi.org/10.1103/PhysRevB.79.224416. URL: http://dx.doi.org/10.1103/PhysRevB.79.224416.

[57] N. Mecking, Y. S. Gui, and C.-M. Hu. "Microwave photovoltage and photoresistance effects in ferromagnetic microstrips". In: *Phys. Rev. B* 76.22 (2007). DOI: http://dx.doi.org/10.1103/PhysRevB.76.224430. URL: http://dx.doi.org/10.1103/PhysRevB.76.224430.

[58] Andrei Slavin and Vasil Tiberkevich. "Spin Wave Mode Excited by Spin-Polarized Current in a Magnetic Nanocontact is a Standing Self-Localized Wave Bullet". In: *Phys. Rev. Lett.* 95.23 (2005). DOI: 10.1103/PhysRevLett.95.237201. URL: http://dx.doi.org/10.1103/PhysRevLett.95.237201.

[59] C. Bayer et al. "Spin-wave excitations in finite rectangular elements of Ni 80 Fe 20". In: *Phys. Rev. B* 72.6 (2005). DOI: http://dx.doi.org/10.1103/PhysRevB.72.064427. URL: http://dx.doi.org/10.1103/PhysRevB.72.064427.

[60] J. P. Park et al. "Spatially Resolved Dynamics of Localized Spin-Wave Modes in Ferromagnetic Wires". In: *Phys. Rev. Lett.* 89.27 (2002). DOI: 10.1103/PhysRevLett.89.277201. URL: http://dx.doi.org/10.1103/PhysRevLett.89.277201.

[61] R. D. McMichael and B. B. Maranville. "Edge saturation fields and dynamic edge modes in ideal and nonideal magnetic film edges". In: *Phys. Rev. B* 74.2 (2006). DOI: http://dx.doi.org/10.1103/PhysRevB.74.024424. URL: http://dx.doi.org/10.1103/PhysRevB.74.024424.

[62] I. N. Krivorotov et al. "Temperature Dependence of Spin-Transfer-Induced Switching of Nanomagnets". In: *Phys. Rev. Lett.* 93.16 (2004). DOI: http://dx.doi.org/10.1103/PhysRevLett.93.166603. URL: http://dx.doi.org/10.1103/PhysRevLett.93.166603.

[63] James O. Rantschler et al. "Surface anisotropy of permalloy in NMNiFeNM multilayers". In: *J. Appl. Phys.* 97.10 (2005), 10J113. DOI: http://dx.doi.org/10.1063/1.1853711. URL: http://dx.doi.org/10.1063/1.1853711.

[64] Hans T. Nembach et al. "Mode- and Size-Dependent Landau-Lifshitz Damping in Magnetic Nanostructures: Evidence for Nonlocal Damping". In: *Phys. Rev. Lett.* 110.11 (2013). DOI: http://dx.doi.org/10.1103/PhysRevLett.110.117201. URL: http://dx.doi.org/10.1103/PhysRevLett.110.117201.

[65] R. E. De Wames. "Dipole-Exchange Spin Waves in Ferromagnetic Films". In: *J. Appl. Phys.* 41.3 (1970), p. 987. DOI: http://dx.doi.org/10.1063/1.1659049. URL: http://dx.doi.org/10.1063/1.1659049.

[66] S.O. Demokritov and V.E. Demidov. "Micro-Brillouin Light Scattering Spectroscopy of Magnetic Nanostructures". In: *IEEE Trans. Magn.* 44.1 (2008), pp. 6–12. DOI: 10.1109/TMAG.2007.910227. URL: http://dx.doi.org/10.1109/TMAG.2007.910227.

[67] Henning Ulrichs et al. "Parametric excitation of eigenmodes in microscopic magnetic dots". In: *Phys. Rev. B* 84.9 (2011). DOI: http://dx.doi.org/10.1103/PhysRevB.84.094401. URL: http://dx.doi.org/10.1103/PhysRevB.84.094401.

[68] Philippe Djemia, François Ganot, and Philippe Moch. "Brillouin scattering in ultrathin permalloy films: monolayers and multilayers with alumina interfaces". In: *Journal of Magnetism and Magnetic Materials* 165.1-3 (1997), pp. 428–430. DOI: http://dx.doi.org/10.1016/S0304-8853(96)00577-X. URL: http://dx.doi.org/10.1016/S0304-8853(96)00577-X.

[69] A.Z. Maksymowicz et al. "Exchange constant and surface pinning in single permalloy films". In: *Thin Solid Films* 197.1-2 (1991), pp. 287–292. DOI: 10.1016/0040-6090(91)90239-T. URL: http://dx.doi.org/10.1016/0040-6090(91)90239-T.

[70] Neil Smith, David Markham, and David LaTourette. "Magnetoresistive measurement of the exchange constant in varied-thickness permalloy films". In: *J. Appl. Phys.* 65.11 (1989), p. 4362. DOI: http://dx.doi.org/10.1063/1.343273. URL: http://dx.doi.org/10.1063/1.343273.

[71] A. Helmer et al. "Quantized spin-wave modes in magnetic tunnel junction nanopillars". In: *Phys. Rev. B* 81.9 (2010). DOI: http://dx.doi.org/10.1103/PhysRevB.81.094416. URL: http://dx.doi.org/10.1103/PhysRevB.81.094416.

[72] J. P. Nibarger et al. “Variation of magnetization and the Lande g factor with thickness in Ni–Fe films”. In: *Appl. Phys. Lett.* 83.1 (2003), p. 93. DOI: http://dx.doi.org/10.1063/1.1588734. URL: http://dx.doi.org/10.1063/1.1588734.

[73] G. Venkat et al. “Proposal for a Standard Micromagnetic Problem: Spin Wave Dispersion in a Magnonic Waveguide”. In: *IEEE Trans. Magn.* 49.1 (2013), pp. 524–529. DOI: 10.1109/TMAG.2012.2206820. URL: http://dx.doi.org/10.1109/TMAG.2012.2206820.

[74] S Mizukami, Y Ando, and T Miyazaki. “Ferromagnetic resonance linewidth for NM/80NiFe/NM films (NM=Cu, Ta, Pd and Pt)”. In: *Journal of Magnetism and Magnetic Materials* 226-230 (2001), pp. 1640–1642. DOI: http://dx.doi.org/10.1016/S0304-8853(00)01097-0. URL: http://dx.doi.org/10.1016/S0304-8853(00)01097-0.

[75] G. D. Fuchs et al. “Spin-torque ferromagnetic resonance measurements of damping in nanomagnets”. In: *Appl. Phys. Lett.* 91.6 (2007), p. 062507. DOI: http://dx.doi.org/10.1063/1.2768000. URL: http://dx.doi.org/10.1063/1.2768000.

Chapter 4

Conclusion

It is widely known that spin-polarized current can excite self-oscillations in 0D systems where the ferromagnetic layer is constricted. Recent work in 2D systems where the ferromagnetic layer is a thin flm with no added constriction has shown that self-oscillations are not possible but rather reduces the saturation magnetization[54]. This thesis explored the 1D case by using a ferromagnetic wire and showed that self-oscillations do occur[27]. The modes excited were shown to be the bulk and edge spin wave eigenmodes where fine splitting occurred due to confinement from the leads by using spin torque ferromangetic resonance, self-oscillatory emission measurements, micromagnetics, and micro Brillouin light scattering. This new dimensionality for spin torque oscillators needs to be studied further to better understand what exactly inhibits self-oscillatory dynamics.